RESEARCH ARTICLE

Spatiotemporal assessment of the nexus between urban sprawl and land surface temperature as microclimatic effect: implications for urban planning

Ahmed Ali A. Shohan[1] · Hoang Thi Hang[2] · Mohammed J. Alshayeb[1] · Ahmed Ali Bindajam[1]

Abstract

Rapid urbanisation has led to significant environmental and climatic changes worldwide, especially in urban heat islands where increased land surface temperature (LST) poses a major challenge to sustainable urban living. In the city of Abha in southwestern Saudi Arabia, a region experiencing rapid urban growth, the impact of such expansion on LST and the resulting microclimatic changes are still poorly understood. This study aims to explore the dynamics of urban sprawl and its direct impact on LST to provide important insights for urban planning and climate change mitigation strategies. Using the random forest (RF) algorithm optimised for land use and land cover (LULC) mapping, LULC models were derived that had an overall accuracy of 87.70%, 86.27% and 93.53% for 1990, 2000 and 2020, respectively. The mono-window algorithm facilitated the derivation of LST, while Markovian transition matrices and spatial linear regression models assessed LULC dynamics and LST trends. Notably, built-up areas grew from 69.40 km^2 in 1990 to 338.74 km^2 in 2020, while LST in urban areas showed a pronounced warming trend, with temperatures increasing from an average of 43.71 °C in 1990 to 50.46 °C in 2020. Six landscape fragmentation indices were then calculated for urban areas over three decades. The results show that the Largest Patch Index (LPI) increases from 22.78 in 1990 to 65.24 in 2020, and the number of patches (NP) escalates from 2,531 in 1990 to an impressive 10,710 in 2020. Further regression analyses highlighted the morphological changes in the cities and attributed almost 97% of the LST variability to these urban patch dynamics. In addition, water bodies showed a cooling trend with a temperature decrease from 33.76 °C in 2000 to 29.69 °C in 2020, suggesting an anthropogenic influence. The conclusion emphasises the urgent need for sustainable urban planning to counteract the warming trends associated with urban sprawl and promote climate resilience.

✉ Hoang Thi Hang
   hlhangstac@gmail.com

   Ahmed Ali A. Shohan
   ashohan@kku.edu.sa

   Mohammed J. Alshayeb
   malshayeb@kku.edu.sa

   Ahmed Ali Bindajam
   abindajam@kku.edu.sa

[1] Department of Architecture and Planning, College of Engineering, King Khalid University, Abha, Kingdom of Saudi Arabia

[2] Department of Geography, Faculty of Natural Science, Jamia Millia Islamia, New Delhi, India

Introduction

Accelerating global urbanisation is changing land use and land cover (LULC) and has a significant impact on urban areas, where an estimated 80% population growth is expected by 2050 (Nath et al. 2021; Seyam et al. 2023; Talukdar et al. 2020; Naikoo et al. 2020; Malanson and Alftine 2023; Yao et al. 2023). This expansion leads to a decline in green vegetation, which is crucial for maintaining the climatic balance (Rahaman et al., 2022; Mahmood et al. 2014; Zhang et al. 2018; Gunawardena et al 2017; Moazzam et al. 2022), and drives up land surface temperatures (LST), which is an important issue in urban environmental studies (Shahfahad et al. 2023a; Lal et al. 2022; Thakur et al. 2021). The complicated relationship between LULC changes and

LST dynamics is further complicated by factors such as regional climate, topography and urban design and requires advanced methods for a better understanding of these phenomena (Shahfahad et al. 2021; Garg and Anand 2022 ; Namgyal et al. 2023; Imran et al. 2021; Hou and Du 2020).

Through the use of remote sensing technologies, researchers can now observe urban environments in unprecedented detail utilizing satellite images like Landsat 8's TIRS and MODIS to study LST variations in different LULC classes (Talukdar et al 2020; Wulder et al 2018; Tsagkatakis et al 2019; Shahfahad et al 2021; AlDousari et al 2022; Gerace et al 2020; Yang et al 2023; Kabir et al 2023; Almeida et al 2021; Elfarkh et al 2020). The spatial dynamics of LULC, especially in urban areas, are critical to understanding the broader ecological impacts of urbanisation, including the 'edge effect' on LST and the need for scenario-based urban management strategies (Chakraborti et al 2019; Shen et al 2022; Derdouri et al 2021; He et al 2023; Ignatieva et al 2011; Mohamed et al 2020; Talukdar et al 2021; Bartesaghi-Koc et al 2022; Yonaba et al 2023; Guo et al 2015; Mendes and Prevedello 2020; Zhang et al., 2022; Zhou et al 2017; Li et al 2014). However, despite the abundance of data, there is a lack of precision to explore the complexity of interactions between LULCand LST due to the lack of sophisticated techniques (Aryal et al. 2023; Singh et al. 2021). These technologies facilitate the study of the effects of urban sprawl on LST and fulfil the need for in-depth studies on the variability of LST in cities and the impact of urban fragmentation on LST (Zhang et al., 2022; Shahfahad et al. 2021).

Recent literature emphasises the importance of machine learning in LULC mapping (Ouma et al. 2022; Shetty 2019; Sarkar et al. 2021) and highlights its potential to improve the accuracy and efficiency of LULC classification. Recent advances in machine learning have enabled innovative approaches for mapping and analysing LULC with high precision, providing insights into urban sprawl and its environmental impacts (Aryal et al. 2023; Singh et al. 2021; Ouma et al. 2022; Jamali 2020). These methods enable the classification of complex urban landscapes and the monitoring of their evolution over time, which is helpful in the management and mitigation of urban heat islands (Shetty 2019; Srivastava et al. 2022; Krivoguz et al. 2023; Loukika et al. 2021; Wang et al. 2022).

In addition, a deeper understanding of LST fluctuations and the factors influencing them is crucial for sustainable urban planning. Studies have shown that urbanisation leads to significant changes in LST, with impacts varying in different regions and at different time scales (Farid et al. 2022; Roy et al. 2020; Mukherjee and Singh 2020; Saleem et al. 2020; Srikanth and Swain 2022). Advanced remote sensing and thermal imaging techniques have become indispensable tools in this research, providing valuable data for assessing the impact of LULC on LST and guiding urban development to minimise negative thermal impacts (Ermida et al. 2020; Guha and Govil 2022; Sekertekin and Bonafoni 2020; Yang et al. 2020; Li et al. 2023).

The intricate interplay between the spatial configurations of LULC and LST is a focus of dynamic research and is influenced by a variety of factors, including regional climate, topography, the characteristics of individual land patches and the cooling effect of green tree canopies (Chakraborti et al. 2019; Shen et al. 2022; Derdouri et al. 2021; An et al. 2022). These elements emphasise the need for state-of-the-art methods for LULC classification, LST extraction and simulation modelling to deepen our understanding of their complex relationship (Shahfahad et al. 2021; Garg et al., 2022; Namgyal et al. 2023). Moreover, the spatial dynamics of LULC, especially in urban environments, have broader ecological implications that extend beyond their immediate surroundings. Concepts derived from landscape ecology such as the edge effect and 'neighbouring features' play a crucial role in how urban change influences LST, requiring a nuanced analysis of these factors and their broader ecological impacts (He et al. 2023; Ignatieva et al. 2011; Mohamed et al. 2020; Talukdar et al. 2021; Bartesaghi-Koc et al. 2022; Yonaba et al. 2023). Innovative approaches are used to explore these dynamics and gain insights for sustainable urban planning by establishing the relationship between urban sprawl and LST variations (Shahfahad et al. 2023b; Phelps and Nichols (2022); Guo et al 2015; Mendes and Prevedello 2020; Zhang et al., 2022; Zhou et al 2017; Li et al 2014). This comprehensive approach aims to untangle the complex web of interactions between LULC and LST and pave the way for sound urban development strategies that mitigate the negative thermal impacts.

However, while a large number of studies have shed light on the impact of urban sprawl on seasonal and annual LST, the subtleties of the impact of urbanisation on inter-annual LST variability in cities need to be investigated in more detail (Zhang et al., 2022; Shahfahad et al 2021; Li et al., 2022; Zhou et al 2011; Su et al 2021). As the influence of urban sprawl on LST can vary depending on regional characteristics, there is a clear need for advanced studies on urban sprawl and LST dynamics. While the temporal evolution of LULC patterns and their influence on LST are well studied, there are still gaps in understanding the complex spatial heterogeneity of urban landscapes (Gerace et al. 2020; Namgyal et al. 2023; Mohamed et al. 2020; Shahfahad et al. 2023a & b). The current literature has not adequately addressed how specific LULC classes, particularly in terms of urban fragmentation, influence LST in different geographical contexts (Yang et al. 2023; Zhang et al., 2022; Zhou et al. 2017; Furlan et al. 2022). In addition, many studies do not use advanced statistical methods to establish causal relationships between LULC

classes and LST. The exact influence of urban areas, their fragmentation patterns and the corresponding effects on neighbourhood LST need to be further investigated.

The main objective of this study is to decipher the multi-layered relationship between urbanisation (in particular the fragmentation and growth patterns of built-up areas) and the microclimatic changes it induces, with a focus on LST. Through the use of a range of landscape metrics, the study aims to quantify urban sprawl, its fragmentation dynamics and the resulting changes in LST over three crucial decades. Furthermore, the study seeks to assess the accuracy and reliability of the LULC models developed using the random forest (RF) algorithm to ensure that subsequent analyses are soundly based. Furthermore, the study aims to provide a probabilistic assessment of possible transitions between different LULC classes and thus provide a predictive insight into the future landscape dynamics of the city.

The present study is ground-breaking in its approach to understanding the intricate relationship between the urban landscape and local surface temperature dynamics, especially in the context of the city of Abha. This research uses machine learning, specifically the RF algorithm, with advanced statistical tools to create a synergistic model to analyse the LULC-LST relationships. Unlike previous studies, which often relied on isolated methods, this research takes a holistic viewpoint. By transforming the traditional LULC data into a binary format, the research has focussed exclusively on built-up areas. This allows for a detailed assessment of urban sprawl and its climatic impacts at the micro level. This increased focus on urban landscapes, which differs from broader landscape analyses, provides unprecedented granularity for understanding urban heat dynamics. By focusing on urban fragmentation indices and their evolution over time, the study goes beyond general urbanisation metrics and sheds light on the nuanced ways in which urban morphology influences thermal behaviour. Essentially, the novelty lies in the in-depth examination of how specific fragmentation patterns and urban morphologies, quantified by customised landscape metrics, correlate with and potentially drive changes in LST.

Given the detailed examination of urban fragmentation and its thermal impacts, it is hypothesised that regions experiencing rapid urbanisation, especially those characterised by increased fragmentation, will experience a significant increase in LST. This thermal increase is likely to be more pronounced in fragmented urban areas compared to other LULC classes. The underlying assumption behind the study is that the degree and type of urban fragmentation, as captured by specific landscape metrics, will have a direct and measurable influence on LST dynamics. The research assumes that a causal relationship exists where nuanced urban patches, especially those characterised by specific fragmentation features, play a central role in shaping LST dynamics.

Materials and methods

Study area

The semi-arid region of Asir, Saudi Arabia, encompasses four major cities: Abha, Khamis Mushayet, Alwadean and Ahad Rufaida. This area is situated in the southwestern part of Saudi Arabia, which is the largest country in the Middle East. Asir spans an area of 2286.59 square kilometres and is located between latitudes 17°59′21.452″N and 18°30′33.812″N, as well as longitudes 42°18′56.269″E and 42°56′25.909″E (Fig. 1). The terrain of the study area is characterized by rolling hills, with elevations ranging from 1038 to 2990 m above sea level, averaging at 2180 m. Annual rainfall in this region averages 355 mm, primarily occurring between April and June. The typical minimum and maximum temperatures are 18.50 and 31.50 °C, respectively. This area encompasses one of the most diverse and abundant floristic regions within the Asir Mountains. Jabal Al-Sooda, a renowned mountain in the region, stands at 2990 m in the northwestern part of the study area, boasting a rich variety of plant life. The combination of diverse climate and topography in the Asir Province has resulted in a wide array of plant species (Abulfatih 1984). Anthropogenic activities, steep slopes, fragile geology and rainfall contribute to significant land loss and ecological imbalances in the area. Among the four cities, Abha City presently serves as the capital of the Asir region. According to the 2012 census by the General Statistics Authority, Abha City is home to 289,975 people, with Saudis constituting 78% of the population (Bindajam and Mallick 2020). The configuration of these cities, featuring various topographical levels, often leads to urban expansion. The main attractions for visitors to these cities are the scenic mountain vistas. Anticipated substantial urban growth in these four pivotal cities of the Asir region underscores the need for a sustainable approach to urban sprawl and development, aiming to enhance the quality of life for both residents and tourists.

Data source

This research utilized multi-date Landsat satellite imagery from the years 1990, 2000 and 2020 to study landscape changes and land surface temperature (LST) over nearly three decades. The bands of the respective images were combined to create multispectral images for 1990, 2000 and 2020. The details about the Landsat satellite imagery used in the study have been given in Table 1. These images were free from clouds and haze and exhibited good contrast.
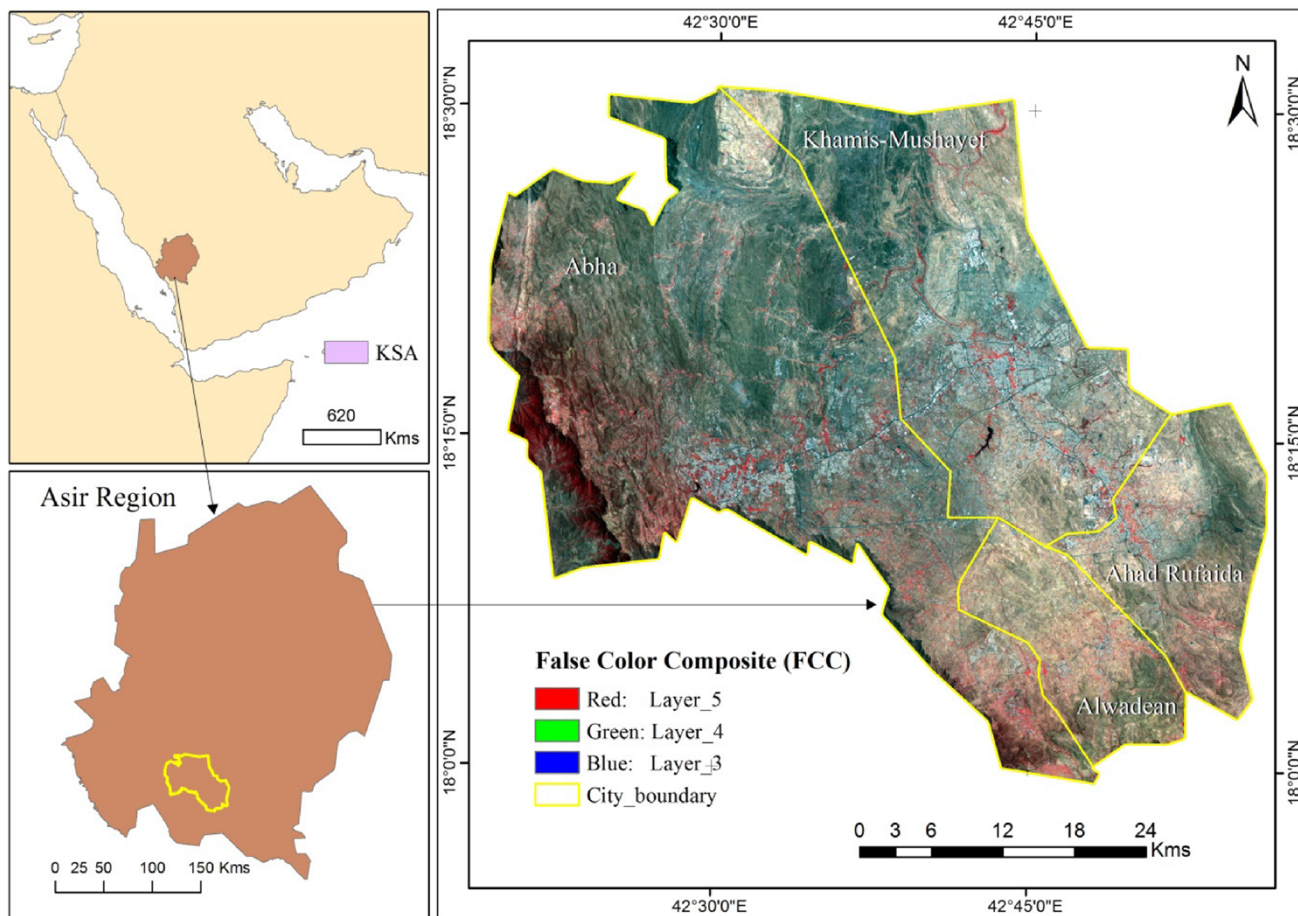
Fig. 1 Study area map of Abha city

Table 1 Details about the satellite data used in the study

S. no	Landsat data	Year	Retrieval time	Resolution
1	Landsat 5 TM	1990	02 Jun 1990	30 m
2	Landsat 5 TM	2000	28 May 2000	30 m
3	Landsat 8 OLI	2020	25 Jun 2020	30 m

Radiometric calibration and geometric registration were carried out and subsequently applied for land use/land cover (LU/LC) extraction. A field survey was conducted from June 20th to July 5th, 2020.

For the analysis, various software tools were employed, including ArcGIS 10.3, TerrSet 19.0.1, earth resources data analysis systems (ERDAS) Imagine 9.2, Fast Line-of-sight atmospheric analysis of spectral hypercubes (FLAASH) 4.8 for GIS and image processing, as well as statistical package for the social sciences (SPSS) 24 for statistical computations. All machine learning data analysis and mapping tasks were performed in a Python integrated Jupyter Notebook environment.

The Garmin-GPS was used for field observations.

Method for LULC mapping using RF

In monitoring and assessing environmental changes, LULC mapping stands as an indispensable tool (Talukdar et al. 2020). The RF algorithm, an ensemble learning technique, has become a linchpin in this domain due to its prowess in managing large, intricate datasets, effectively addressing multicollinearity and missing values and delivering superior classification accuracy (Atef et al. 2023; Talukdar et al. 2020; Rihan et al. 2023). Its core methodology involves the construction of multiple decision trees during training and the subsequent derivation of the mode of the class labels by individual trees for the final classification prediction (Wang et al. 2019). When deployed on satellite or aerial imagery datasets, such as those sourced from Landsat or Sentinel, the RF classifier leverages spectral values, texture metrics and any available ancillary data to differentiate between various LULC classes. For LULC classification of Abha city spanning the years 1990, 2000 and 2020, multispectral and multitemporal datasets have been distinctly processed with the RF algorithm. To further bolster the classifier's performance, hyper-parameter tuning is essential. The inherent robustness

of the RF algorithm can be amplified by optimising hyper-parameters like the number of trees (n_estimators), tree max depth (max_depth) and the requisite minimum samples for node splitting (min_samples_split). Grid Search, a prevalent hyper-parameter tuning technique, facilitates the exhaustive exploration of a predefined hyper-parameter space, evaluating model efficacy for each combination via cross-validation. Applying this to Abha city's LULC mapping, a parameter grid for RF hyper-parameters has been defined, and through grid search coupled with cross-validation, the optimal parameter set is determined. The ensuing model, trained on the entirety of the dataset with these optimal parameters, assures a pinnacle of classification accuracy for the LULC mapping across the specified years.

Method for accuracy assessment of LULC

Land use and land cover map (LULC) accuracy assessment, which is crucial for evaluating the quality of map classification (Chughtai et al. 2021; Naikoo et al. 2020), involves comparing field surveys and Google Earth–derived reference patterns with the map values to derive key metrics. For the LULC mapping of the city of Abha using an optimised random forest (RF) model, the study uses a confusion matrix to distinguish between actual and classified categories and to highlight omission errors (false negatives) and walk-in errors (false positives). The user's accuracy per class measures the probability of correct pixel classification on the map, while the producer's accuracy evaluates the correct classification of ground truth pixels. The overall accuracy and the kappa coefficient, which compares the observed accuracy to chance, provide a detailed performance evaluation of the RF model for the 1990, 2000 and 2020 datasets for the city of Abha.

Method for LST estimation

Land surface temperature (LST) plays a crucial role in understanding local climatic variations, urban heat islands and many ecological processes (Sumanta 2022; Gohain et al. 2023; Moazzam et al. 2022; Naikoo et al. 2022a, b; Mokarram et al. 2023; Mallick et al. 2008). Satellite remote sensing provides an efficient means to retrieve LST on a regional scale (Xu et al. 2023). The urban heat island (UHI) formation has been estimated using the Simulated Single Image (SSI) method, which integrates statistical analysis of LANDSAT time series data to map urban hot spots and UHI development (Corumluoglu 2023). Further, the Mono-Window (MW) algorithm is one of the widely employed techniques for LST retrieval from thermal infrared (TIR) remote sensing data (Shahfahad et al. 2023a; Wang et al. 2015; Sekertekin and Bonafoni 2020). The fundamental premise of the Mono-Window Technique is based on the

radiative transfer equation, which relates at-satellite radiance to ground emissivity and LST. Firstly, the at-satellite brightness temperature (Tb) is derived from the digital numbers or radiance values of the thermal band. This requires sensor-specific calibration constants that convert the observed values into radiance and subsequently into brightness temperature using the Planck function.

However, the brightness temperature alone is not sufficient for a true representation of LST, given the influences of atmospheric effects, especially water vapour. The Mono-Window Technique, therefore, incorporates an atmospheric correction, which usually requires knowledge about atmospheric water vapour content and the mean atmospheric temperature. The LST estimation using the Mono-Window algorithm is given by:

$$LST = \frac{Tb}{1 + (\omega^* \lambda^* Tb / \rho) * \ln(\varepsilon)} \tag{1}$$

where Tb is the at-satellite brightness temperature; ω represents the effective mean atmospheric temperature; λ is the wavelength of emitted radiance, typically around 11.5 μm for most thermal infrared sensors; ρ is the Boltzmann constant, and ε is the emissivity of the land surface, which can vary based on the surface type.

For the estimation of LST in Abha city for the years 1990, 2000 and 2020, multispectral datasets that contain thermal infrared bands are necessary. For Landsat 4–5 TM, the thermal band (Band 6) captures data between 10.40 and 12.50 μm, whereas for Landsat 8 OLI, the thermal bands (Band 10 and 11) operate in the 10.60–11.19-μm and 11.50–12.51-μm ranges, respectively. After obtaining the brightness temperatures for each of these years, the Mono-Window Technique can be applied by incorporating site-specific and date-specific atmospheric parameters. Additionally, for a city like Abha with diverse land cover, it might be necessary to have an emissivity map, which can be derived from the LULC map itself or other methods, to accurately represent the spatial variations in emissivity across the city.

Temporal evolution of LULC using change matrix and Markovian transition probability

The temporal analysis of land use and land cover patterns (LULC) is of crucial importance for sound urban planning and nature conservation. Change matrix and Markovian transition probability methods are used to track changes over time (Naikoo et al 2020; Chen et al 2022; Talukdar et al 2021; Naikoo et al. 2022a, b; Bindajam et al 2023). The change matrix visualises the LULC transitions between two periods by capturing shifts from one class to another, with diagonal elements indicating stability and non-diagonal elements indicating change. The Markov approach, which is

based on the premise that future LULC states depend solely on the current state, uses transition probabilities to forecast future LULC scenarios and thus helps in strategic environmental and urban development planning. This concise summary highlights the methods' contributions to understanding LULC dynamics over time and facilitates sustainable management practises.

Temporal evolution of LST using spatial linear regression model

Analysing the temporal evolution of LST provides insights into the changing thermal characteristics of a landscape (Zhou et al. 2011; Zhang et al., 2022; Li et al. 2014). A spatial linear regression model enables a pixel-wise study of how LST has evolved over different time periods. Such an approach allows us to account for the spatial heterogeneity inherent in urban landscapes, where various factors—ranging from urban infrastructure, green spaces, water bodies, to land use changes—can lead to diverse local thermal responses. The rationale behind this study lies in the recognition that Land Surface Temperature (LST) values at individual spatial points (pixels) can be affected by a range of both human-induced and natural factors, making it crucial to comprehend the pace and trend (whether increasing or decreasing) of these changes over time.

In the context of spatial linear regression, a linear regression is conducted for each pixel (i,j) within the study area, employing LST values from multiple time points (specifically, 1990, 2000 and 2020) as the dependent variables and the respective years as independent variables; the resulting output, denoted as the slope for each pixel, provides insight into the rate of LST change per year. The slope, representing the temporal trend, offers valuable information; positive values indicate a rise in land surface temperature (LST) over time, signifying areas undergoing warming potentially attributed to urbanization, deforestation or other land cover alterations, while negative values suggest a decline in LST, implying cooling trends linked to augmented vegetation, reforestation or urban green initiatives. The R-squared statistic, assessing the goodness of fit, quantifies the portion of the variation in the dependent variable (LST) accounted for by the independent variable (years), and elevated values indicate a stronger alignment of the linear model with the data; particularly in LST studies, a high R-squared value may imply that temporal factors, such as alterations in urban layout or land cover, exert substantial influence on LST changes in that specific location. The p value, assessing the significance of the trend, offers a test of the null hypothesis positing no trend (slope equals zero); a low p value (often < 0.05) signifies the ability to reject the null hypothesis, indicating that the trend is statistically significant. Therefore, spatial linear regression on LST provides a granular view of thermal dynamics, capturing the intricacies of local changes and offering a comprehensive perspective on landscape thermal behaviour over time.

Relationship between LULC classes and LST at temporal scale

Understanding the relationship between LULC classes and LST is critical in the domains of urban planning, environmental science and climate studies (Varade et al. 2023; Shahfahad et al. 2023a; Zhou et al. 2014; Ghosh et al. 2022; Pande et al. 2023). This relationship is often non-linear and varies spatially and temporally, with different LULC classes having distinct thermal characteristics (Ghosh et al. 2022; Mallick et al. 2008). Thus, a robust analysis incorporates both zonal statistics for different LULC classes and a statistical examination of temporal changes in LST within these classes.

Zonal statistics for LULC and LST

Zonal statistics serve as a computational method to extract and summarize the spatial characteristics of one dataset (e.g., LST) based on the categorical delineation provided by another (e.g., LULC classes). In the context of assessing LST within LULC classes, the spatial domain of each LULC class is utilized to mask the LST data. This operation effectively filters out LST values that fall within the spatial boundaries of a specific LULC class. Following this, aggregate statistics such as the mean, maximum and minimum LST are computed for this subset of data. By performing this computation iteratively across all unique LULC classes, a profile of LST behaviour within each class is obtained. Furthermore, when this process is replicated for LST datasets from different temporal points (e.g., 1990, 2000, 2020), it elucidates the temporal shifts in LST dynamics within each LULC category, reflecting the influence of land use changes, urbanization, or conservation efforts on surface temperatures.

Temporal LST trends via statistical analysis

To discern the statistical significance and nature of LST variations within each LULC class over time, linear regression and ANOVA are employed. For every LULC class, the mean LST values are regressed against the study years, generating a trend line. The slope of this trend signifies the direction and magnitude of change in LST over time. The coefficient of determination, R^2, quantifies the proportion of variance in LST that can be attributed to the temporal progression, thus serving as a measure of the trend's robustness. Simultaneously, an ANOVA test is conducted on LST values across the years within each LULC class. This assesses whether

the mean LST values differ significantly between the time points. The *F*-value from the ANOVA signifies the ratio of variance between the group means to the variance within the groups, and the associated *p* value gauges the statistical significance of this variance. Together, these statistical tools offer a comprehensive evaluation of LST evolution within the constructs of LULC classes.

Urbanization impact assessment as per landscape fragmentation analysis

Assessing the impact of urbanisation by analysing landscape fragmentation is a crucial method for deciphering the spatial patterns and intensity of urban sprawl (Salvati et al. 2018; Lin et al. 2023; Hu et al. 2022; Talukdar et al. 2021). By reclassifying the LULC maps into binary representations in which built-up areas are isolated, we can track the spatial progression of urbanisation over time (Lin et al. 2023; Salvati et al. 2018; Bindajam et al. 2023; Dewa et al. 2022). Landscape metrics applied to these binary representations provide a quantitative framework for assessing urban growth. The Largest Patch Index (LPI) is calculated by identifying the largest contiguous urban area within the binary landscape matrix. The index is the size of this largest patch expressed as a percentage of the total landscape area. This metric is a direct measure of the dominance of the largest urban fabric and is inversely related to fragmentation; a higher LPI indicates a more consolidated urban landscape. The number of patches (NP) is a simple count of the individual urban patches within the landscape. An increase in NP over time indicates a fragmented landscape in which urban areas are increasingly dispersed and disjointed (Zhou et al. 2022; Wu et al. 2022; Li et al. 2022; Azabdaftari and Sunar 2022). Patch density (PD) is determined by dividing the NP by the total area of the landscape. This is a measure of density that reflects the degree of fragmentation and the intensity of urban sprawl. A higher PD indicates a more fragmented urban structure, with numerous small patches scattered across the landscape. The landscape shape index (LSI) is derived by examining the shapes of individual urban areas and comparing them to a standard geometric shape, usually a square or circle. The LSI is calculated by dividing the total perimeter of the patch by the square root of the total area of the landscape and then comparing this value to a neutral shape index of the same area. This metric measures the complexity and irregularity of urban patch shapes, with higher values indicating more irregular urban shapes (Tang et al. 2023). Mean patch area (MPA) is the average size of individual urban patches and is calculated by dividing the total urban area by the NP. It provides an indication of the extent of urbanisation, with larger average sizes indicating fewer and larger urban areas and smaller sizes indicating a more granular and fragmented urban pattern (Tian et al.

2022). The fractal dimension (FD) is a measure of the complexity of form resulting from the ratio of perimeter to area of urban areas. It is calculated according to the following formula:

$$FD = 2 * log(NP) / log(Area)$$

This index provides a dimensionless value that captures the complexity of urban patch shapes. Values closer to 1 indicate simple, smooth patch perimeters, while values closer to 2 indicate highly complex, convoluted patch shapes characteristic of sprawling urban development (Kotrosits 2013).

Calculating these metrics allows for a temporal and spatial comparison of landscape structure, allowing patterns and trends in urbanisation to be identified. By applying these metrics to binary maps across different points in time, researchers can quantify and visualise the dynamic process of urban growth and its impact on the landscape.

Temporal dynamics of urban fragmentation

Analysing these metrics across time, specifically for the years 1990, 2000 and 2020, can uncover temporal patterns of urban evolution. A rise in LPI over the years might signify a trend towards urban consolidation or the emergence of mega urban clusters. On the other hand, an increasing trend in NP and PD would indicate a progression towards more fragmented urban landscapes. An augmenting LSI would reflect increasingly irregular urban shapes, possibly due to haphazard development or encroachments into non-urban zones. These temporal patterns, captured by the fragmentation metrics, offer quantitative foundations to urban change narratives, linking back to driving forces like policy shifts, economic trends or population dynamics.

Statistical interpretation of urbanization and LST correlation

Upon obtaining these landscape metrics, it becomes pivotal to statistically assess their relationship with the LST. Employing linear regression techniques, it is feasible to ascertain the strength and significance of associations between landscape fragmentation indicators and LST. For instance, a positive regression slope between FD and LST would suggest that as urban areas become more complex (or fragmented), there is a corresponding rise in LST. The R^2 value from the regression delineates how much of the LST variation can be explained by changes in a specific fragmentation metric. A significant *p* value would further confirm that the observed relationships are unlikely due to random chance. Thus, through rigorous statistical tests, the intricate interplay between urbanization patterns and LST can be

deciphered, providing a robust basis for urban planning and policy-making endeavours.

The entire methodology employed in this study is illustrated in Fig. 2.

Results

Temporal LULC mapping and accuracy assessment

LULC modeling using RF model

The application of a Grid Search optimized RF model for LULC mapping of Abha city for the years 1990, 2000 and 2020 revealed distinct optimal hyper-parameters for each period. For 1990, the model preferred a relatively moderate tree depth (max_depth: 25) with a higher number of trees (n_estimators: 150). These parameters, combined with 'auto' for max_features (which equates to the square root of the number of features), indicate a balanced trade-off between model complexity and generalization. The scenario in 2000 demonstrated a slight inclination for deeper trees (max_depth: 30) and a more conservative approach to node splitting, as indicated by min_samples_split: 5 and min_samples_leaf: 2, which ensures a more pronounced reduction in overfitting. Conversely, for the 2020 mapping, there was a surge in the number of trees (n_estimators: 200) with a return to the 1990's tree depth, suggesting potentially richer or more varied data inputs, warranting a more robust forest. The consistent use of auto for max_features across all years underscores the stability in data dimensionality and the algorithm's preference for considering a subset of features at

Fig. 2 A comprehensive flowchart depicting the methodologies employed for the spatiotemporal assessment of urban sprawl and its influence on LST in the context of urban planning
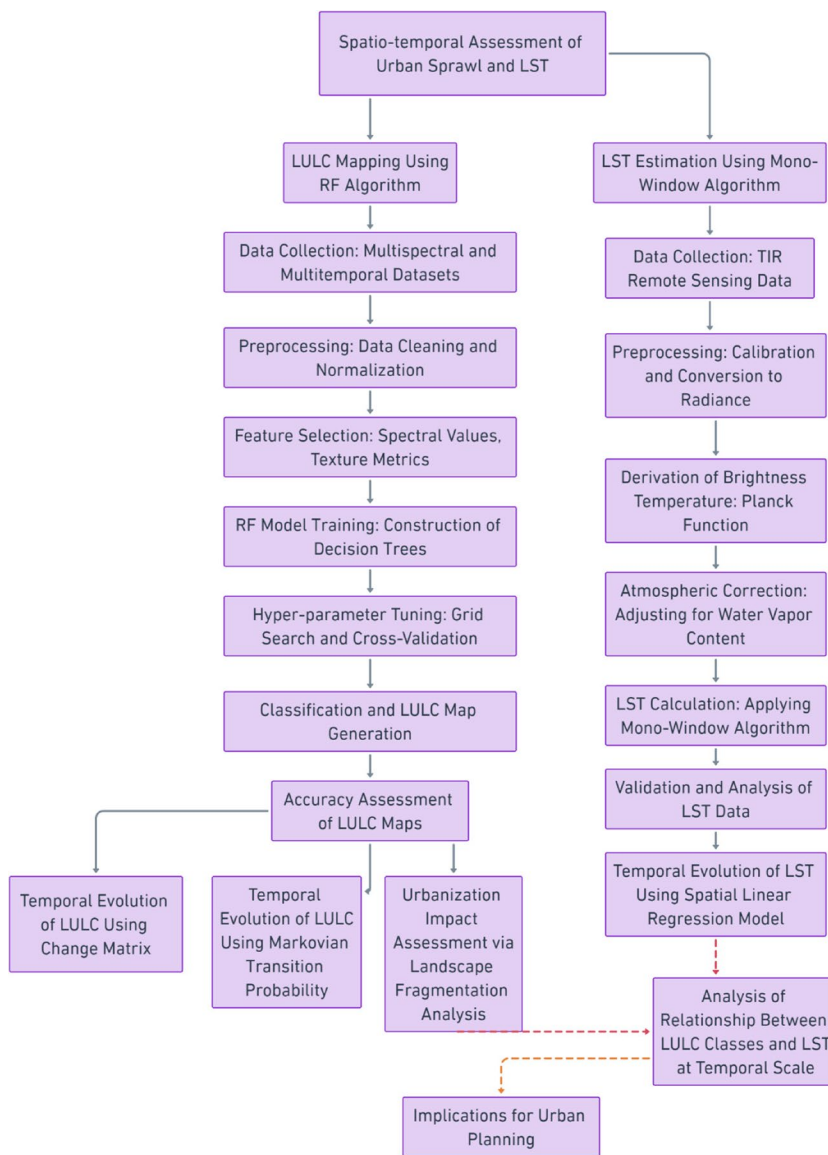
each split. When applied to the diverse LULC classes such as built-up, water body and various vegetation types, among others, these hyper-parameters ensure precise and accurate mapping, capturing the city's nuanced environmental and urban dynamics over the three-decade span.

Accuracy assessment of the LULC models

The RF-based LULC models for Abha city over the years 1990, 2000 and 2020 have demonstrated a commendable level of accuracy when assessed against reference datasets. The models, while generally consistent, revealed some nuanced variations across different classes and years. Evaluating LULC with precision against ground truth data is paramount.

In 1990, the overall accuracy was 89.99% with a kappa coefficient of 0.8843, reflecting a high degree of reliability. User accuracy for categories such as built-up and exposed rock was high, with values above 0.89, meaning that most users would correctly identify these classes (Supplementary Table 1 and 2). However, for water bodies, user accuracy was lower at 0.67474, indicating some confusion in identifying the classes. Producer accuracy was above 0.82 for most classes, with water bodies and exposed rocks scoring above 0.95, indicating a high probability that these classes were correctly identified. In 2000, overall accuracy increased slightly to 90.15% with a kappa coefficient of 0.8862. In this year, user accuracy improved for built-up areas and dense vegetation with values above 0.91, indicating that users were more likely to correctly identify these classes (Supplementary Table 3 and 4). Producer accuracy remained high for water bodies and exposed rocks, also above 0.97. In 2020, the accuracy assessment showed the best performance with an overall accuracy of 91.72% and a kappa coefficient of 0.9043 (Supplementary Table 5 and 6). In particular, user accuracy for built-up areas increased to 0.952484 and for water bodies improved significantly to 0.793522. Producer accuracy for agricultural land and exposed rocks was particularly high at 0.91 and 0.979 respectively, indicating a very accurate representation of these classes in the LULC map. Commission errors remained relatively low for all classes and years, although some categories such as water bodies in 1990 and sparse vegetation in 2000 and 2020 had higher values. Omission errors were also low, with the highest errors observed in sparse vegetation in 1990 and 2000. The consistent reduction in omission errors by 2020 for most classes indicates an improvement in the completeness of the classification over time. In all years, user accuracy was high for most LULC classes, especially for built-up areas and exposed rocks, suggesting that map data users were able to identify these categories with high confidence. Producer accuracy was also high, particularly for water bodies and exposed

rocks, confirming the precision of these classifications in the map. The low commission and omission errors for most classes across all years confirm the robustness of the classification, although some classes had higher errors, indicating areas for future improvement. The increasing trend in overall accuracy and kappa values over the years shows that LULC classification techniques and data quality have improved over time.

Land use land cover classification results

The LULC patterns, as illustrated in Fig. 3, present the spatial distribution of distinct land cover types over three distinct periods: 1990, 2000 and 2020, derived using the RF algorithm. The quantitative representation of these patterns is tabulated in Table 2, which meticulously computes the areal extent of each LULC class across the three observation years. From Table 2, we discern several noteworthy trends and shifts in LULC dynamics over the three-decade span. There is an evident expansion of built-up regions, growing from 69.40 km^2 in 1990 to a substantial 338.74 km^2 by 2020. This threefold increase underscores rapid urbanization or infrastructural development in the area under study. The area encompassed by water bodies has seen a decline, contracting from 1.51 km^2 in 1990 to just 0.54 km^2 in 2020, which could be indicative of water bodies being subjected to anthropogenic pressures or changes in hydrological patterns. Dense vegetation has experienced a gradual increase over the years, expanding from 43.36 km^2 in 1990 to 52.22 km^2 in 2020. Conversely, sparse vegetation demonstrated a dip in 2000 (193.52 km^2) but rebounded in 2020 to 237.21 km^2, suggesting potential shifts between dense and sparse vegetation classifications or land management practices. Croplands have witnessed fluctuations, with an initial expansion from 105.24 km^2 in 1990 to 135.03 km^2 in 2000, followed by a significant reduction to 64.76 km^2 by 2020. This could be attributed to changes in land use practices, urban encroachment or alterations in agricultural policy. Scrubland, constituting a major portion of the land, experienced a decrease from 1032.72 km^2 in 1990 to 785.58 km^2 in 2000 and a slight resurgence to 827.35 km^2 in 2020. Bare soils, on the other hand, peaked in 2000 at 353.57 km^2 but reduced substantially by 2020 to 186.14 km^2. Exposed rocks showed a consistent increase till 2000 but witnessed a slight decline by 2020.

Therefore, the LULC dynamics, as visualized in Fig. 3 and quantified in Table 2, portray a landscape undergoing considerable transformations, with burgeoning urban areas, fluctuating vegetation and changes in natural terrains. These shifts, reflective of both anthropogenic interventions and natural processes, offer critical insights for land management, urban planning and environmental conservation efforts.
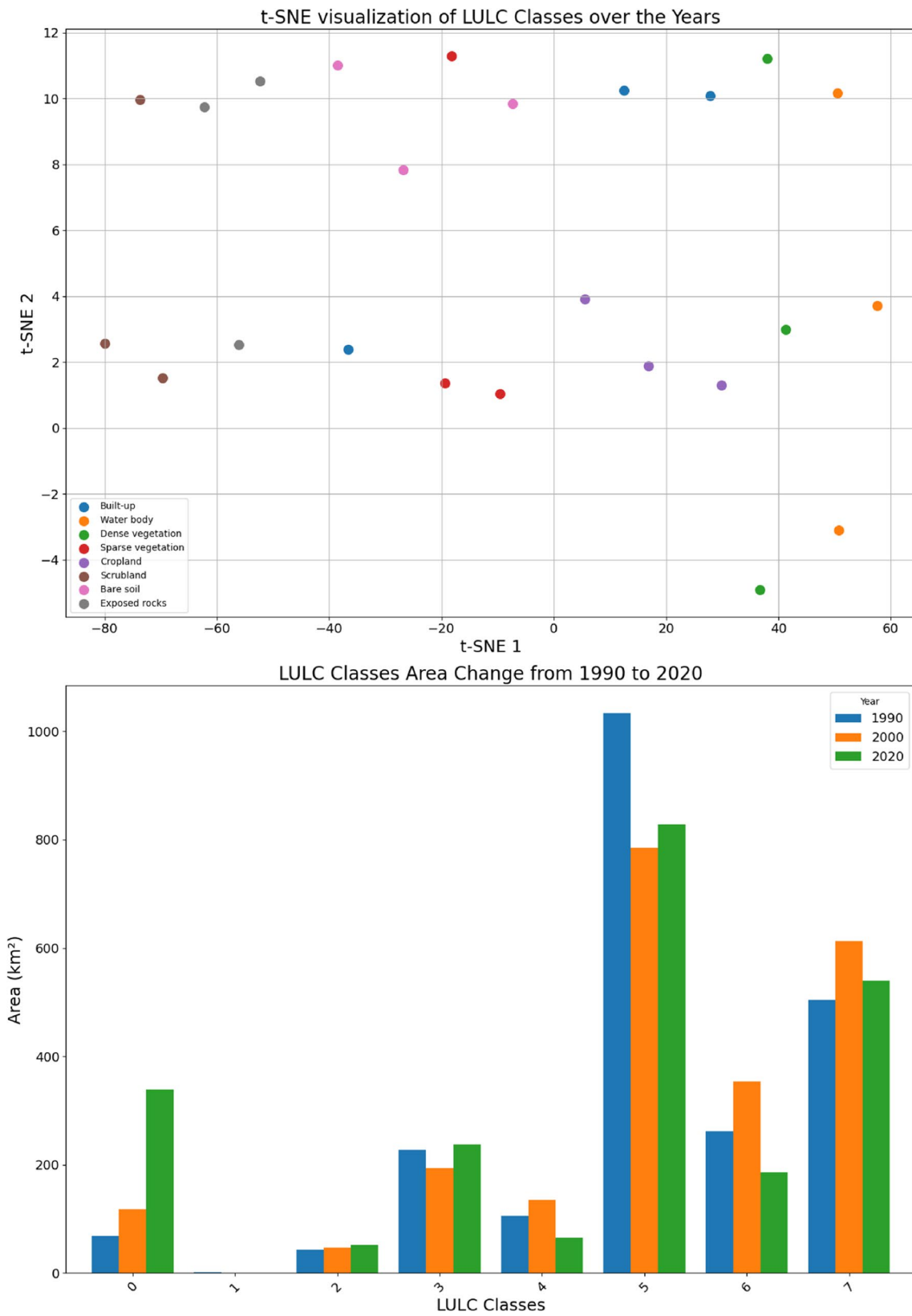
Fig. 3 Distribution and divergence of various land cover types over time

Table 2 Area (in km^2) under different LULC categories

LULC classes	Areas in (km^2)		
	1990	2000	2020
Built-up	69.40	117.60	338.74
Water body	1.51	1.14	0.54
Dense vegetation	43.36	47.23	52.22
Sparse vegetation	228.46	193.52	237.21
Cropland	105.24	135.03	64.76
Scrubland	1032.72	785.58	827.35
Bare soil	262.31	353.57	186.14
Exposed rocks	503.57	612.90	539.62

Land surface temperature results

LST data extracted from Landsat 4–5 TM and Landsat 8 OLI imagery show a pronounced change in the thermal landscape of the city of Abha over three decades. The LST images were first validated with ground-based measurements (Supplementary Table 7), which confirmed the reliability of the satellite observations. The field observations conducted in June 2018 showed a high correlation with the satellite-derived LST, indicating that the temporal evolution of the LST is consistent with the in situ data. In particular, the Landsat 4–5 TM and Landsat 8 OLI-derived LST values agreed well with the ground-based measurements: dense vegetation at 35.40 °C versus 33.05 °C, built-up concrete at 47.35 °C versus 45.50 °C, asphalt at 56.75 °C versus 54.60 °C and exposed rocky areas at 53.70 °C versus 52.60 °C. This validation emphasises the credibility of our satellite-based LST analysis. The temporal trajectory of LST spanning three decades, as depicted in Fig. 5, underscores marked alterations in the region's thermal milieu. Leveraging the mono-window algorithm, satellite imageries from Landsat 4–5 TM for 1990 and 2000, juxtaposed with Landsat 8 OLI data for 2020, facilitated these LST derivations. In 1990, the first year of observation, the land surface temperature (LST) values ranged from a low of 16.74 °C to a high of 58.58 °C, defining the thermal range of the area. In 2000, the thermal boundary had shifted, and the LST values ranged from a minimum of 19.50 °C to a maximum of
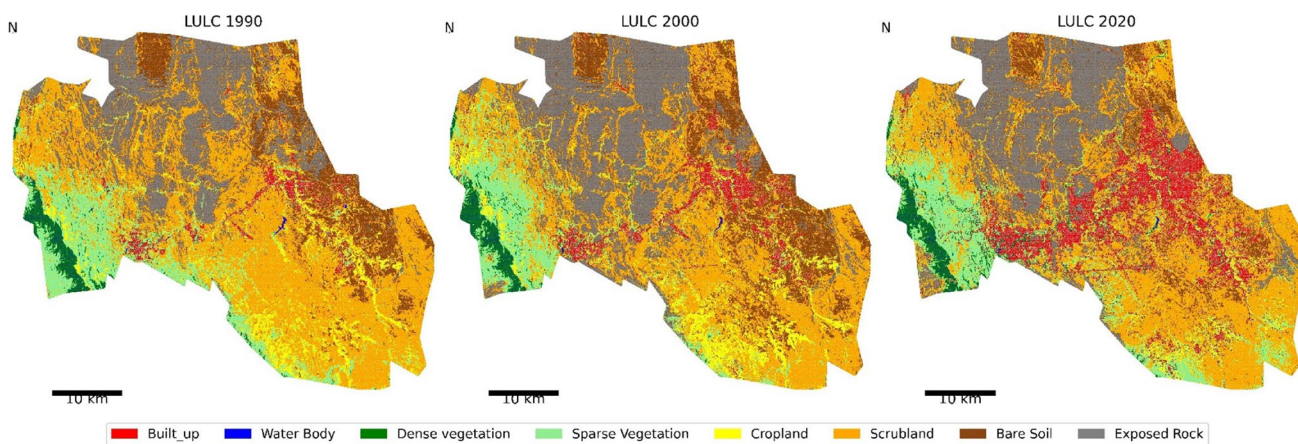

Fig. 4 Spatial representation of land use and land cover (LULC) classes for the years 1990, 2000 and 2020
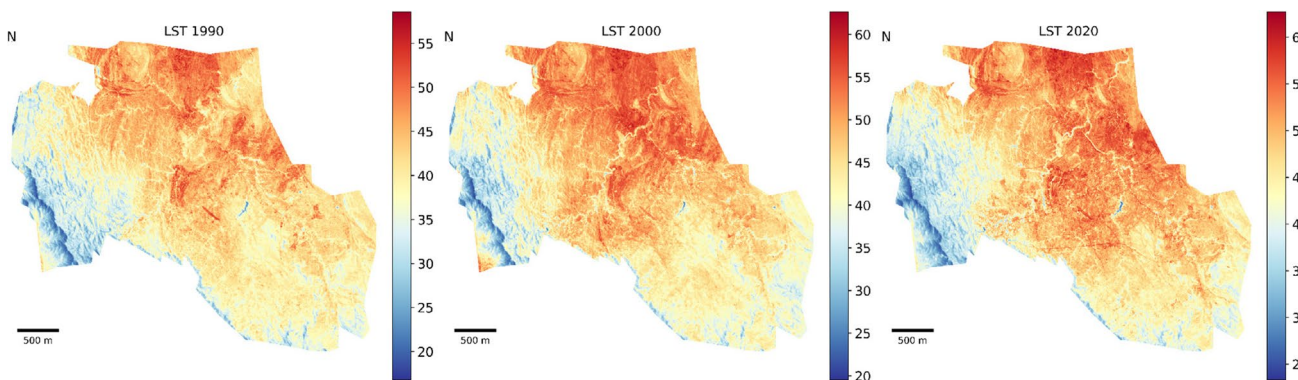

Fig. 5 Spatial distribution of land surface temperature (LST) for the years: 1990, 2000 and 2020

62.63 °C. In 2020, the thermal profile continued to evolve, with temperatures ranging from 23.29 °C at the lowest to 62.70 °C at the highest.

A spatial analysis shows that the western ends of the city, which are equipped with vegetation, consistently had LST values of below 30 °C. Remarkably, this vegetative footprint, which acts as a heat buffer, has decreased over the years, in line with the expansion of built-up areas. In contrast, the northern quadrant of the city, which is predominantly characterised by rocks and barren terrain, is a hotspot with temperatures consistently above 45 °C, and this thermal intensity is on a rising trajectory. The core of the city, stretching from the eastern to the central zone, is home to Abha's main urban conglomerate. In this area, the LST has intensified and frequently exceeds the 48 °C mark. As urban sprawl has increased, so have the regions where temperatures above 48 °C are recorded. This emphasises the urban heat island effect and the impact of urban expansion on the local heat regime. A clear increase in the extent of exposed rock can be seen in Figs. 3 and 4 between 1990 and 2020, which appears to correspond to an increase in LST over the same period. This correlation suggests that the decrease in vegetation cover and the subsequent increase in exposed rock could contribute to an increase in local temperatures. Exposed rock surfaces naturally have a lower albedo than vegetation, meaning that they reflect less solar radiation and absorb more heat, leading to higher observed temperatures in these areas. Such changes in land cover not only affect local thermal profiles, but can also have wider ecological and environmental impacts, including altered microclimates and potentially negative impacts on biodiversity. The parallel trends highlighted in these figures emphasise the critical interaction between land cover and regional climate dynamics (Fig. 5).

Land use land cover dynamics

In this study, we used change matrix and Markovian transitional probability analysis to explore the urban dynamics over 30-year span. The change matrix provided in Fig. 6 offer a granular insight into the nuanced shifts and dynamics of the LULC over a span of three decades. The initial decade highlighted the burgeoning urban footprint. Built-up areas expanded notably by approximately 49.58 km^2 from its original state. This urban sprawl predominantly encroached upon scrublands (8.82 km^2), exposed rocks (7.52 km^2) and bare soils (2.47 km^2). Water bodies exhibited a commendable resilience with retention of approximately 0.92 km^2, with only minor transitions from built-up (0.03 km^2) and dense vegetation areas (0.04 km^2). Sparse vegetation, accounting for about 124.27 km^2, was in a dynamic state, showcasing significant interchange with scrublands (49.81 km^2) and exposed rocks (30.70 km^2).

The period from 2000 to 2020 further emphasised the urban expansion narrative. Built-up areas surged dramatically, capturing an additional 96.52 km^2 of the landscape. A significant portion of this expansion occurred at the expense of scrublands, which saw a reduction of about 89.00 km^2 transitioning to urban territories. Moreover, croplands, which spanned 34.23 km^2, also underwent a substantial metamorphosis, primarily converting into and out of scrublands (49.07 km^2). The 30-year overview accentuates the macroscopic LULC dynamics. Urban (built-up) regions burgeoned predominantly by annexing territories from scrublands, bare soils and exposed rocks. The dense vegetation largely maintained its integrity, spanning around 37.15 km^2, with only minor areas transitioning to and from sparse vegetation (8.07 km^2). Sparse vegetation, covering 117.87 km^2, exhibited fluidity, especially with scrublands (43.32 km^2). Croplands, over the three decades, oscillated primarily with scrublands, with an interchange of about 49.07 km^2.

Therefore, the LULC transition matrices present a landscape undergoing profound transformations. The relentless urban expansion, especially at the expense of natural habitats like scrublands and exposed rocks, underscores the anthropogenic pressures. This comprehensive, quantitative assessment accentuates the need for sustainable urban planning and conservation strategies to balance development and ecological preservation.

The Markovian transition matrices in Fig. 6 provide a probabilistic assessment of the potential transitions between different LULC classes over two distinct intervals: 2000–2020 and 1990–2020. Examining the data from Fig. 6, urban (built-up) regions showcased a high-retention probability of 82.08% over the two decades. This indicates a predominant stability in urban areas, with minor expansions primarily at the expense of scrublands (9.33%) and exposed rocks (3.83%). Water bodies demonstrated a retention probability of 43.65%, but also showed a significant transition potential to dense vegetation (23.99%). Dense vegetation areas exhibited a substantial stability with a 78.64% retention probability, with the most significant outflux to sparse vegetation (17.09%). Sparse vegetation, with a 60.91% retention probability, experienced notable transitions to scrublands (22.39%). Croplands, while maintaining a 25.35% retention probability, showed a strong inclination to transition into scrublands (36.34%). Scrublands and exposed rocks, with retention probabilities of 66.76% and 73.59% respectively, showed the most stable dynamics in this period.

The cumulative transition matrix over three decades, as elucidated in Fig. 6, reiterates many of the trends observed in the 2000–2020 interval. Built-up areas maintained a dominant stability, with a 82.08% retention probability. The most significant flux from this category was towards scrublands (9.33%). Water bodies, despite a moderate retention probability of 43.65%, showed a marked
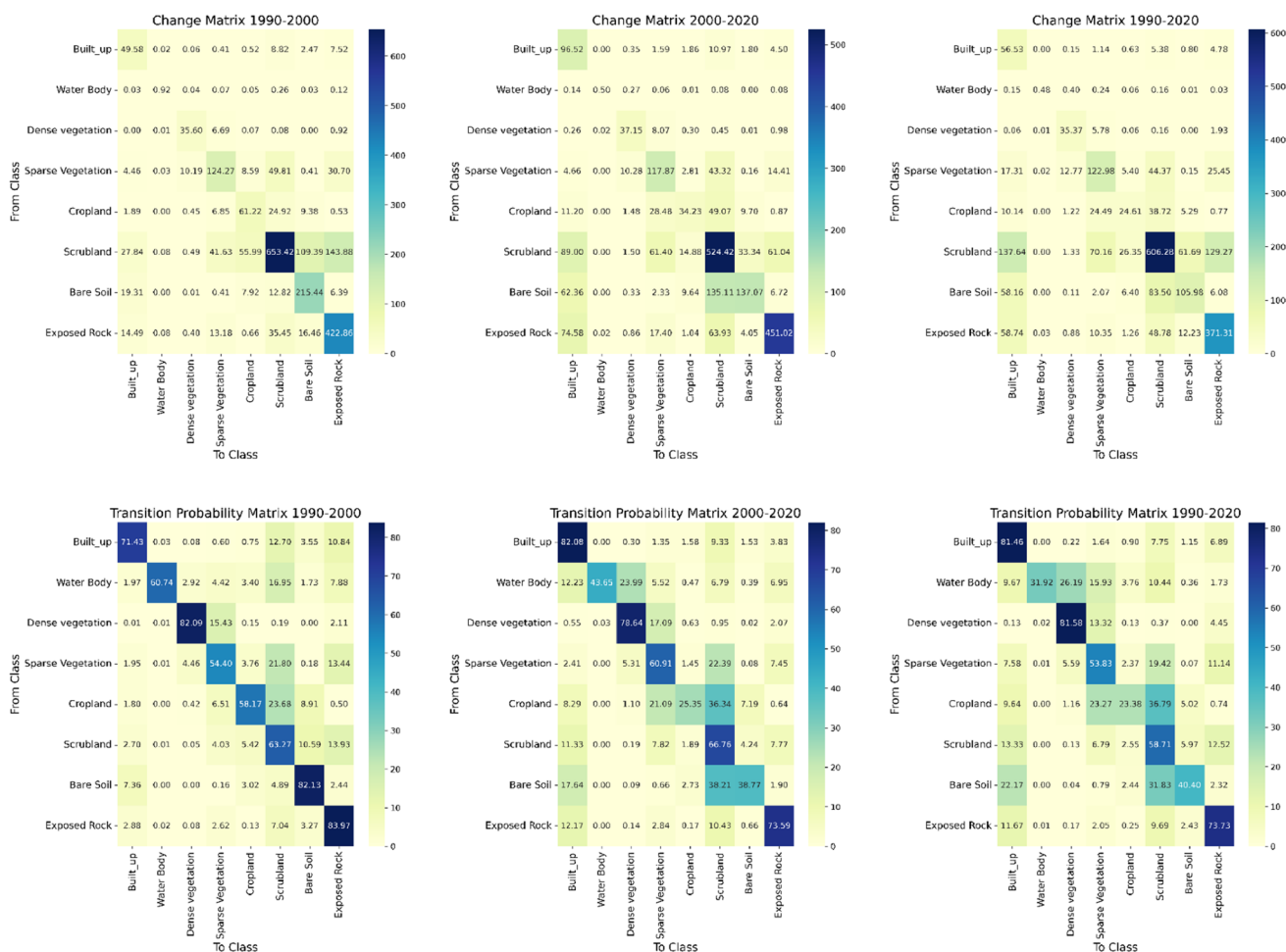
Fig. 6 LULC change and transition matrices for 1990–2000, 2000–2020 and 1990–2020

tendency to morph into dense vegetation (23.99%). Dense and sparse vegetations largely mirrored the trends from the previous interval, with retention probabilities of 78.64% and 60.91%, respectively. Croplands and scrublands continued their trend, with croplands leaning towards transitioning into scrublands (36.34%) and scrublands maintaining a retention probability of 66.76%. Bare soils and exposed rocks, with retention probabilities of 38.77% and 73.59%, respectively, indicated the landscape's inertia against rapid changes in these classes.

The change matrices and transitional probability assessments offer a rigorous, quantitative insight into the multi-decadal evolution of the landscape. These analyses underscore the dynamic interplay between anthropogenic influences and natural processes, revealing persistent patterns of urban expansion, habitat alterations and the relative stabilities of various land cover classes over time.

Assessment of LST dynamics

The assessment of LST trends over time is pivotal for understanding the intricate interplay between anthropogenic influences and natural processes. To understand deeper into these temporal dynamics, a spatial linear regression model was implemented at the granular pixel level. This approach enables the capture of nuanced, site-specific thermal variations, offering a detailed insight into the landscape's evolving thermal profile and the driving factors behind these changes. The model's strength lies in its ability to quantify three essential metrics: the slope (indicating trend magnitude and directionality), R^2 (representing the goodness of fit) and the p value (denoting statistical significance). Together, these metrics serve as a comprehensive toolkit, elucidating the magnitude, consistency and significance of LST dynamics across diverse landscapes.
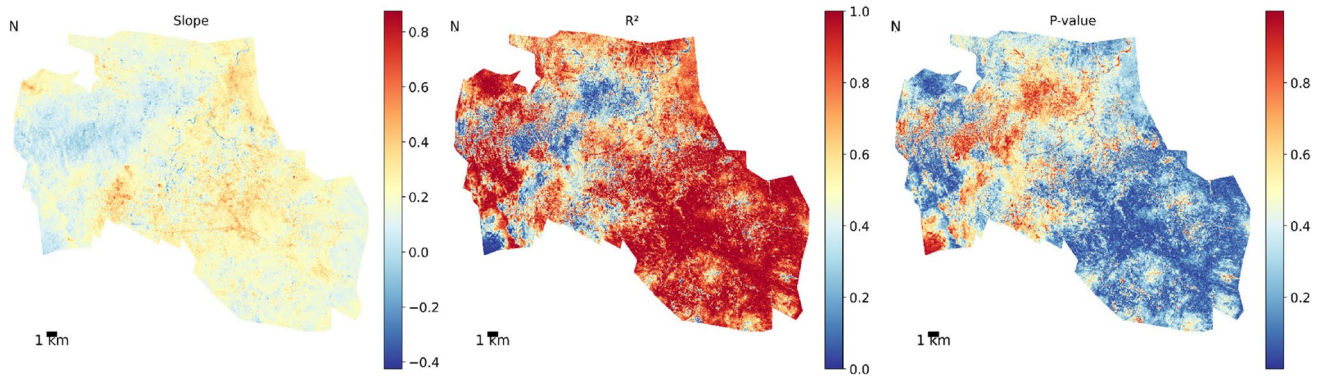
Fig. 7 Detailed spatial linear regression analysis of temporal LST trends using (slope), goodness of fit ($R.^2$) and statistical significance (p value)

The slope or gradient of the regression line represents the rate of change in LST over the temporal scale. From Fig. 7, it is discernible that the study area, especially the urban regions radiating from the middle to the eastern parts, manifests an approximate positive slope, suggesting a warming trend of around 1–2 °C per decade. This is emblematic of the urban heat island effect, a phenomenon where urban areas experience elevated temperatures due to human activities and modifications to the land surface. In contrast, the extreme western part, which is predominantly forested, exhibits a relatively stable or slightly increasing trend, with an approximate slope of 0.5 °C per decade. The northern regions, dominated by bare soil and rocky surfaces, also indicate an increasing LST trend, potentially attributable to the inherent low albedo of such surfaces and the absence of vegetation cover.

Regions in the urban belt, especially those spreading towards the eastern parts, display an R^2 value of approximately 0.6 or higher. This suggests that over 50% of the variability in LST in these regions can be accounted for by the temporal factor alone. The forested regions in the extreme west, while showing a lower trend magnitude, also demonstrate a moderately high R^2 value, indicating a consistent, albeit slower, temperature change.

The p value sheds light on the statistical significance of the observed trends. From the plots, it is evident that the urban areas, especially those expanding towards the east and the west, exhibit p values lower than 0.05. This signifies that the warming trends in these regions are statistically significant and unlikely due to random variations. The northern regions, dominated by rocky surfaces and bare soil, also manifest statistically significant warming trends, with p values approximating 0.05 or lower.

Combining the insights from the trend magnitude, R^2 values and p values, certain patterns emerge. The urban areas, especially those sprawling towards the eastern and western fringes, are undergoing rapid warming. This warming is not only statistically significant but also accounts for a major portion of the LST variability. The forested regions in the west, despite their slower temperature increase, exhibit consistent trends, underlining the subtle influences of deforestation or land-use changes. The northern terrains, with their rocky surfaces, further corroborate the importance of vegetation in modulating LST, as their barrenness results in marked and significant warming trends.

Assessing the relationship between LULC classes and LST at temporal scale

The interplay between LULC changes and LST dynamics stands as a cornerstone in understanding the ecological and climatic shifts of a region. To unravel this intricate relationship, zonal statistics and statistical tests have been employed, offering a detailed quantification and correlation between LULC classes and their consequent LST values over time.

Table 3 presents a comprehensive overview of the LST's temporal dynamics across various LULC classes over three decades. One striking observation is the evident increase in average LST values for built-up areas, which have risen from 43.71 °C in 1990 to 50.46 °C in 2020. This increment can be attributed to factors such as urban heat island effects, increased anthropogenic activities and infrastructural developments in urban regions. Such trends are indicative of the growing thermal footprint of urbanization. Water bodies, which generally serve as thermal sinks, interestingly showcase a decrease in average LST from 33.762 °C in 2000 to 29.695 °C in 2020. This decline might be a reflection of changes in the volume or quality of water bodies, variations in aquatic vegetation or fluctuations in inflow-outflow dynamics. Dense vegetation areas, typically associated with cooler temperatures due to evapotranspiration processes, have also witnessed an increment in average LST from 25.168 °C in 1990 to 32.283 °C in 2020. Such an uptick might be indicative of possible deforestation, land degradation or other anthropogenic pressures reducing the cooling effect of these zones.

Table 3 Zonal statistics illustrating the relationship between LULC classes and their corresponding LST values for the years 1990, 2000 and 2020

| LULC classes	Built-up	Water body	Dense vegetation	Sparse vegetation	Cropland	Scrubland	Bare soil	Exposed rocks
Average_1990	43.710	27.718	25.168	33.546	37.238	40.272	42.659	44.798
Maximum_1990	54.980	43.185	42.093	52.988	49.900	55.212	55.434	58.581
Minimum_1990	25.636	19.411	16.743	19.038	21.547	21.840	26.043	19.917
Average_2000	48.376	33.762	29.621	36.847	40.415	44.353	46.494	49.724
Maximum_2000	59.606	57.738	57.728	54.524	54.902	60.867	58.631	62.635
Minimum_2000	28.305	21.841	19.495	21.882	23.230	24.454	29.350	24.865
Average_2020	50.460	29.695	32.283	39.294	43.309	45.911	49.555	49.769
Maximum_2020	61.729	46.559	57.249	59.672	59.703	61.299	59.878	62.701
Minimum_2020	26.565	25.524	23.292	25.265	27.270	27.765	29.665	26.198
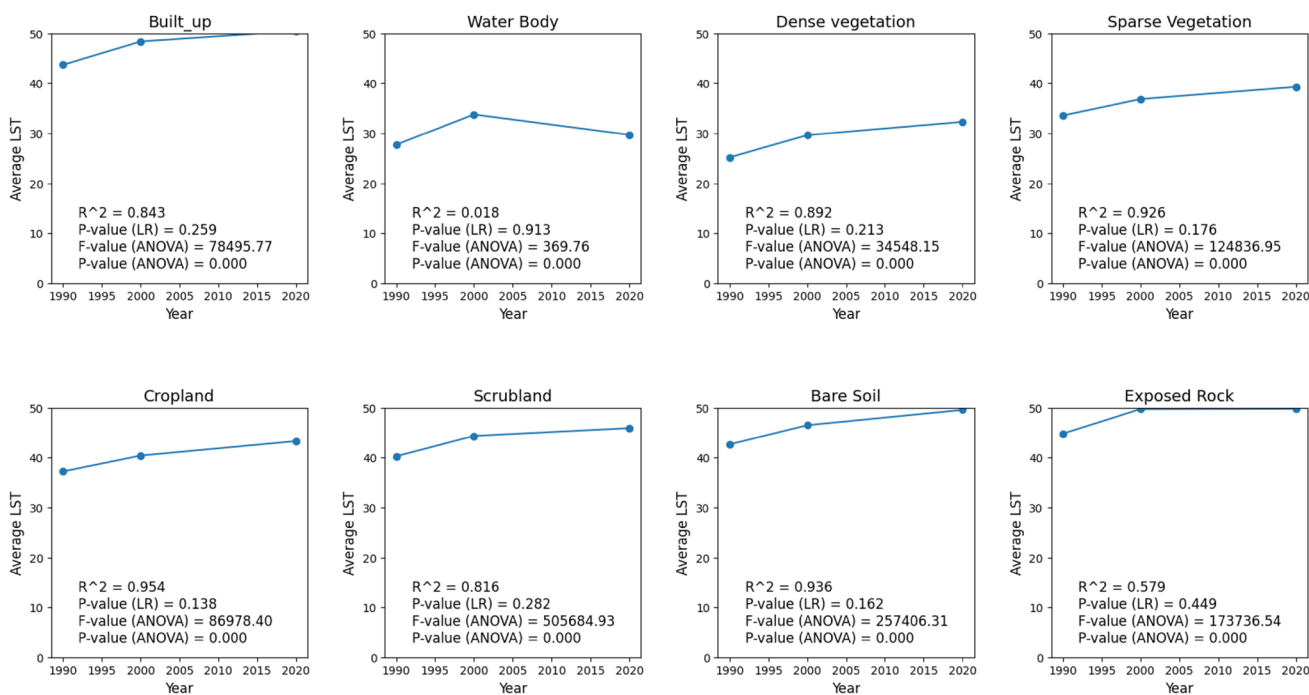
Fig. 8 Results of statistical tests delineating the correlation and significance of LST changes in response to LULC transformations over time

The statistical parameters from Fig. 8 further shed light on the relationship between LULC and LST. The R^2 values, which represent the proportion of LST variability explained by LULC changes, are notably high for certain classes. Built-up areas have an R^2 of approximately 0.843, suggesting that around 84.3% of the variation in LST within these areas can be attributed to changes in the built-up class. Similarly, dense vegetation and sparse vegetation classes have R^2 values of 0.892 and 0.926 respectively, further underscoring the strong correlation between LULC changes and LST dynamics in these regions.

Moreover, the F-values from the ANOVA tests indicate the statistical significance of these relationships. All LULC classes have p values close to 0, highlighting the fact that the observed relationships between LULC and LST are statistically significant and not due to random chance.

Geographically, the directionality of these changes is also crucial. In the extreme western part, which is primarily a forested region, the LST has been consistently cooler. However, as urban areas radiate from the middle to the eastern parts, an increase in LST is evident, with heightened values often exceeding 48 °C. The northern regions, dominated by bare soil and rocky surfaces, also exhibit elevated LSTs, often surpassing 45 °C. Over time, these high LST zones have expanded, signalling an escalation in land surface warming, potentially exacerbated by diminishing vegetative cover and increasing built-up zones. Therefore, based on these results, we decided to study further on only urban landscape how

different arrangements of urban landscape have influence LST.

Urbanization impact assessment based on landscape fragmentation analysis

Built-up area extraction and associated LST dynamics

Analysing the impacts of urbanization on local climate dynamics is paramount in the realm of urban ecology and planning. A novel approach in this study is the meticulous dissection of urban sprawl's fragmentation patterns and their subsequent influence on LST. By transforming the LULC data into a binary format (visualized in Fig. 9), we exclusively focused on built-up areas, enabling a detailed assessment of urbanization's micro-scale impacts. This narrowed perspective enhances the precision of the evaluation, especially when using fragmentation indices in conjunction with LST.

The histograms highlight the frequency distribution of LST within urban patches over three distinct years. In the 1990 histogram, the LST distribution appears to be skewed towards cooler temperatures, with the peak frequency observed around approximately 28 °C (Fig. 10). This suggests that a significant portion of the urban areas had

relatively cooler temperatures during this year. By 2000, the histogram showcases a slight shift towards warmer temperatures, with the most frequent LSTs gravitating around 32 °C. This could be indicative of urban heat island effects intensifying due to increased built-up areas or reduced vegetation. By 2020, the histogram takes on a broader distribution, hinting at a greater variability in urban temperatures. The peak frequency seems to have shifted further to around 34 °C, emphasizing the continued warming trend. However, the broader spread also suggests diverse microclimates within the urban patches, potentially due to factors like urban planning, the introduction of green spaces or variations in building materials.

Fragmentation analysis

Over the span of three decades, the urban landscape of the region has undergone substantial transformation, as evident from the fragmentation metrics. The LPI, which measures the size of the largest urban patch as a percentage of the total landscape, has exhibited a noticeable increase, surging from 22.78 in 1990 to 65.24 by 2020. This uptrend suggests a growing dominance of larger urban patches, potentially indicating a fusion of previously isolated urban fragments or the outward expansion of major urban hubs. Concurrently, the
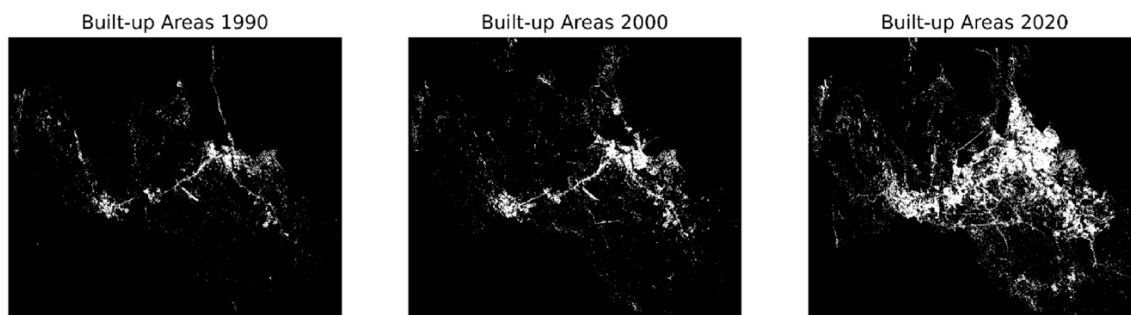

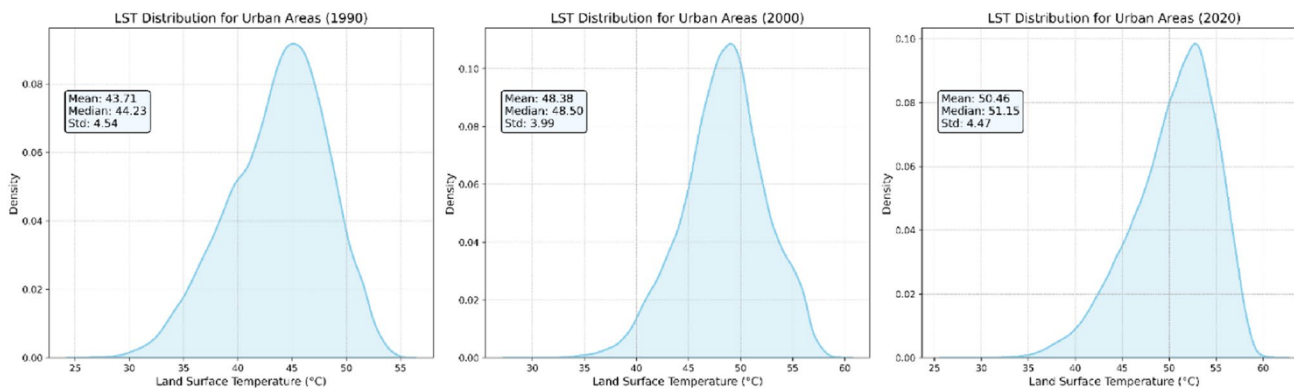**Fig. 9** Spatial distribution of built-up areas

Fig. 10 Frequency distribution of LST within urban patches

NP metric, signifying the count of discrete urban patches, has catapulted from 2531 in 1990 to an impressive 10,710 in 2020.

This substantial increment in LPI highlights the heightened fragmentation and proliferation of urban areas, possibly fuelled by sporadic urban developments, the emergence of satellite towns or infrastructure ventures bisecting existing urban regions. Meanwhile, the MPA offers a slightly contrasting perspective. Its increment from 27,421.73 sq. m in 1990 to 31,628.06 sq. m in 2020, while moderate, suggests that the average size of these burgeoning urban patches has also expanded. This could be attributed to the consolidation of smaller urban fragments or the organic growth of existing ones. The evolution of PD and LSI provides further nuance. A mild decline in PD from 36.467 in 1990 to 31.617 in 2020 indicates a subtle drop in urban patch density. In contrast, the LSI's leap from 57.14 in 1990 to 95.059 in 2020 pinpoints a growing complexity in the shape and configuration of urban patches, a potential repercussion of unchecked urban sprawl or eclectic urban designs.

Statistical analysis

The regression analysis reveals profound insights into the relationship between urban fragmentation and the corresponding variations in LST (Fig. 11). The R^2 values, which signify the proportion of LST variance explained by each metric, are particularly telling. For instance, the LPI, with

an R^2 of 0.97, showcases that approximately 97% of the variability in LST can be explained by the changes in the largest urban patch size. Similarly, the NP and LSI metrics, with R^2 values of 0.96 and 0.98 respectively, affirm their substantial roles in influencing LST dynamics. The slopes of these metrics provide insights into the rate of change over the years. The LPI has a slope of 1.47, suggesting a steady increase in the size of the largest urban patch over the years. In contrast, the NP, with a slope of 283.19, underscores the rapid proliferation of urban patches. The LSI, with its slope of 1.3, also reinforces the growing complexity in urban patch configurations. However, the p values introduce an element of caution. While metrics like LPI, NP and LSI have relatively low p values, suggesting statistically significant relationships, others like MPA ($p = 0.380$) and PD ($p = 0.390$) approach the conventional significance thresholds, hinting at potential nuances or externalities that might be influencing their relationships with LST.

Urban areas, as evidenced by their evolving fragmentation patterns, play a crucial role in modulating local temperature dynamics. The escalating fragmentation and irregularity in urban patches, as indicated by metrics like NP and LSI, can lead to diverse microclimates within a city, influencing local weather patterns, heat stress and urban livability. Among the metrics, LPI, NP and LSI particularly stand out in their capability to elucidate LST dynamics, underscoring the importance of urban planning and design in climate adaptation and resilience. Overall, the regression outcomes
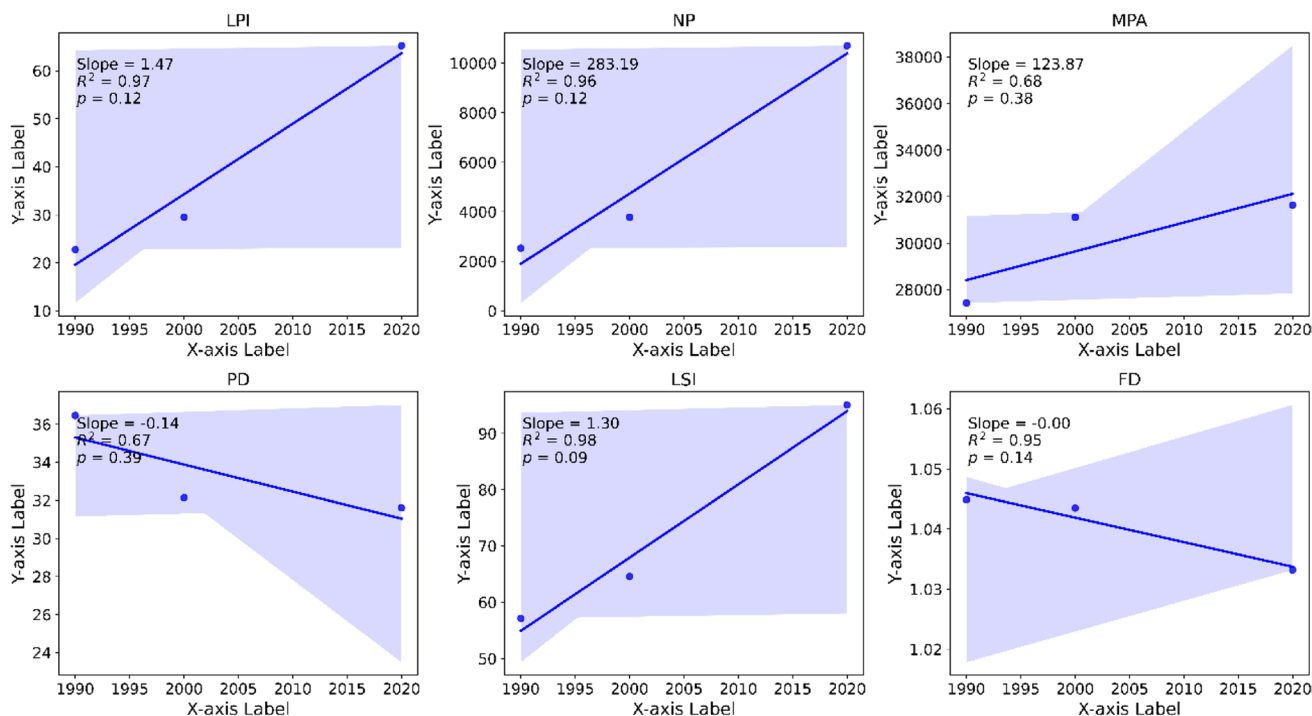

Fig. 11 Temporal trends of selected landscape metrics for the urban built-up areas from 1990 to 2020

highlight the profound influence of urban fragmentation on LST dynamics, underscoring the necessity of sustainable urban planning to mitigate escalating urban temperatures.

Discussion

The intricate interplay between LULC and LST has been the subject of extensive research, especially in the context of urbanization and its resulting environmental effects (Nath et al. 2021; Rahaman et al. 2022). Abha city, in this study, serves as a representative example of many rapidly urbanizing areas, particularly in developing nations, where urban expansion often leads to discernible changes in local microclimates (Moazzam et al. 2022). As the built-up expanse of Abha enlarged nearly fivefold from 69.40 km^2 in 1990 to 338.74 km^2 by 2020, a corresponding uptick in LST to 50.46 °C in 2020 was observed. This trend echoes findings from various other studies where urban growth, characterized by an increase in impervious surfaces, has been directly linked to a rise in LST (Shahfahad et al. 2023a, b; Lal et al. 2022). Abha city's near fivefold increase in built-up areas over three decades underscores a predominant shift towards urban infrastructure, characterized by concrete, asphalt and other man-made surfaces. Such materials typically have high heat capacities and low albedos (Abulibdeh 2021). Consequently, during the day, these surfaces absorb and store more solar radiation compared to natural surfaces. At night, the stored heat is gradually released, leading to elevated temperatures, a phenomenon evident in our study where LST escalated to 50.46 °C in 2020.

This phenomenon aligns with several studies across the globe. For instance, Moisa et al. (2022) observed a similar rise in LST with declining vegetation cover. Vegetation, with its natural ability to provide shade and facilitate evapotranspiration, acts as a cooling agent, reducing LST (Naikoo et al. 2020). As urban areas expand, vegetation is often the first casualty, leading to reduced evapotranspiration and increased heat retention (Zhao et al. 2017). Çorumluoğlu (2023) identified industrial regions, roads, bare lands and certain urban land parts as primary contributors to urban heat islands (UHI) and Urban Hot Spots (UHS) in Izmir. Utilizing the Simulated Single Image (SSI) method, it demonstrated spatial patterns of UHI development influenced by urban land cover and structure types. Additionally, the fragmentation metrics, which highlighted the city's evolving urban morphology, provide insights into the urban structure and layout. A fragmented urban structure, with more patches and edges, can exacerbate heat stress due to increased surface area exposed to solar radiation. Our observation, where the number of patches surged from 2531 in 1990 to 10,710 in 2020, indicates increased fragmentation and potentially

more heat islands within the city. This could be one of the reasons for the substantial increase in LST.

Recent research has established a clear link between changes in land use and land cover (LULC) and land surface temperature (LST). Studies from Seoul to Nanjing show the profound impact of urban development on the local climate. The study from Seoul used advanced artificial intelligence to predict a significant reduction in LST following the conversion of urban areas into green spaces, highlighting the potential of strategic urban planning to combat heat (Kim et al. 2022). Similarly, an analysis in the Dongting Lake emphasised the need for precise LST measurements, linking specific LULC types to different temperature profiles (Tan et al. 2020). Studies in rapidly urbanising regions confirmed the trend and showed a marked increase in LST in response to the loss of vegetation, particularly in autumn. In Nanjing, the cooling effect of croplands and forests was mapped, indicating opportunities to mitigate the effects of the urban heat island (Kaiser et al. 2022). These studies show that land use dynamics are an important factor in LST changes and provide information for sustainable urban management (Wang et al. 2020).

Comparatively, cities with similar geographical and climatic contexts have reported analogous trends. For instance, Alqurashi and Kumar (2019) noted urban expansion-induced LST hikes in cities like Riyadh, Jeddah and Makkah. The commonality in these observations, despite regional nuances, is the profound impact of urban morphology on local thermal dynamics. Furthermore, the inherent topography and microclimatic factors unique to Abha might have compounded the urbanization-induced effects. It is possible that specific geographical or topographical attributes of Abha have a role in the pronounced LST changes. While urbanization is a primary driver, the city's microclimate, influenced by its geographical setting, can either amplify or mitigate the UHI effects. Considering the escalating LST trends, there is a pressing need for Abha's urban planning authorities to prioritize the integration of green infrastructure within city limits. Strategic placement of parks, green roofs, water sprinkle systems and tree-lined streets can mitigate the UHI effect, offering cooler microenvironments and improving overall urban livability. Also, urban planners should prioritize holistic and connected urban layouts over fragmented developments. Ensuring that built-up zones are complemented with contiguous green belts can help in heat dispersion, reducing localized UHI effects. Comparative studies, such as those by Alqurashi and Kumar (2019) and Alqurashi et al. (2016), have noted similar urban-induced LST rise in other Saudi Arabian cities. However, each city has its unique geographical and climatic nuances. Abha's inherent topographical attributes might also influence its microclimate, potentially amplifying urbanization-induced effects. Urban planning should align with the city's

natural geographical attributes. Sloped regions, for instance, can be developed as terraced green spaces, promoting natural cooling.

The hypothesis of the study postulates a direct link between the accelerated urbanisation of the city of Abha and the significant increase in LST, a theory that is confirmed by the results of this study. The almost fivefold increase in built-up areas between 1990 and 2020 is reflected in a significant increase in LST. This supports the hypothesis that urban expansion and the associated increase in impermeable surfaces are major factors in the increased temperatures in cities. This hypothesis is consistent with global research findings linking urban growth to higher LST due to reduced evapotranspiration and increased heat storage by artificial surfaces. The observed fragmentation of urban structure, resulting in increased patchiness and edges, further confirms the hypothesis by showing how urban form can influence microclimatic conditions and potentially contribute to the urban heat island effect. The results of the study argue in favour of urban planning that emphasises green infrastructure to mitigate these thermal effects and are in line with current urban climate resilience strategies.

The results of the study on rapid urbanisation in Abha, Saudi Arabia, and the resulting impact on LST have significant policy implications. The evidence that urban sprawl leads to a significant increase in LST, as shown by the growth of built-up areas and the sharp rise in temperature over three decades, points to the urgent need for integrated urban planning. Policy makers should consider enforcing green building codes that incorporate heat-reflective materials and urban greening initiatives to mitigate the urban heat island effect. The cooling trend observed in water bodies suggests that measures to promote the preservation and enhancement of natural water bodies could be a strategic component of urban climate management. Furthermore, the study's finding that almost 97% of LST variability is due to urban morphology highlights the need for land use planning that prioritises climate resilience. This could include the development of open spaces and the preservation of larger, uninterrupted green spaces in cities to counter fragmentation and promote ecosystem services that cool urban areas. To promote sustainable urban living, urban planners and local governments should implement strategies based on the study's findings. This includes spatial planning that regulates urban expansion, improves green infrastructure and utilises water bodies as natural cooling elements.

Conclusion

The relationship between urban morphology and climatic responses, particularly land surface temperature (LST), has attracted considerable interest in the field of urban ecology and planning. In the rapidly developing city of Abha, this study meticulously mapped the evolution of the urban fabric over three decades, revealing stark changes in the landscape. The land use and land cover (LULC) models built using advanced methods based on the random forest (RF) algorithm showed a robust accuracy of 87.70%, 86.27% and 93.53% for the years 1990, 2000 and 2020, respectively. A strong urban expansion was observed, with the built-up area increasing from 69.40 km^2 in 1990 to 338.74 km^2 in 2020. At the same time, the city's LST dynamics reflected this urban sprawl, with temperatures rising from an average of 43.71 °C in 1990 to a sweltering 50.46 °C in 2020.

These findings emphasise the profound impact of urban growth patterns on local microclimates and reinforce the global discourse on urban heat islands and sustainable urban planning. The novelty of the study is that it focuses on urban landscapes and uses customized landscape metrics to find out how specific urban fragmentation patterns correlate with LST variations. The intricate analysis, particularly of urban sprawl fragmentation patterns and their influence on LST, sets this study apart from others. However, like all scientific endeavours, this study is not without limitations. The time frame, limited to three decades, may overlook longer-term patterns. Furthermore, while the study focuses on the city of Abha, extrapolating the results to other urban contexts should be done with caution due to the different local conditions and urbanization trajectories.

Future research can broaden the temporal and spatial scales and include more diverse urban contexts and longer-term data sets. Given the emerging challenges of climate change, understanding the relationship between cities and LST is crucial. This study paves the way, and it is hoped that researchers around the world will build on this foundation and explore more deeply the multi-layered relationship between urbanization and its climatic impacts to support the formulation of sustainable urban policy.

Author contribution Conceptualization, Ahmed Ali A. Shohan, Hoang Thi Hang, Mohammed J. Alshayeb, Ahmed Ali Bindajam; data curation, Ahmed Ali A. Shohan, Hoang Thi Hang; formal analysis, Ahmed Ali A. Shohan, Hoang Thi Hang; funding acquisition, Mohammed J. Alshayeb; methodology, Ahmed Ali A. Shohan, Hoang Thi Hang; project administration, Mohammed J. Alshayeb, Ahmed Ali Bindajam; resources, Ahmed Ali A. Shohan, Hoang Thi Hang, Mohammed J. Alshayeb, Ahmed Ali Bindajam; software, Hoang Thi Hang; supervision, Mohammed J. Alshayeb, Ahmed Ali Bindajam; validation: Hoang Thi Hang; writing—original draft, Ahmed Ali A. Shohan, Hoang Thi Hang; writing—review and editing, Mohammed J. Alshayeb, Ahmed Ali Bindajam.

Declarations

Ethics approval and consent to participate Not applicable.

Consent for publication Not applicable.

Competing interests The authors declare no competing interests.

References

Abulibdeh A (2021) Analysis of urban heat island characteristics and mitigation strategies for eight arid and semi-arid gulf region cities. Environ Earth Sci 80:1–26

Abulfatih HA (1984) Elevationally restricted floral elements of the Asir Mountains, Saudi Arabia. J arid environ 7(1):35–41

AlDousari AE, Kafy AA, Saha M, Fattah MA, Almulhim AI, Al Rakib A, ... Rahman MM (2022) Modelling the impacts of land use/land cover changing pattern on urban thermal characteristics in Kuwait. Sustain Cities Soc 86:04107

Almeida CRD, Teodoro AC, Gonçalves A (2021) Study of the urban heat island (UHI) using remote sensing data/techniques: a systematic review. Environments 8(10):105

Alqurashi AF, Kumar L (2019) An assessment of the impact of urbanization and land use changes in the fast-growing cities of Saudi Arabia. Geocarto Inte 34(1):78–97

Alqurashi AF, Kumar L, Sinha P (2016) Urban land cover change modelling using time-series satellite images: A case study of urban growth in five cities of Saudi Arabia. Remote Sens 8(10):838

An NN, Nhut HS, Phuong TA et al (2022) Groundwater simulation in Dak Lak province based on MODFLOW model and climate change scenarios. Front Eng Built Environ 2:55–67

Aryal J, Sitaula C, Frery AC (2023) Land use and land cover (LULC) performance modeling using machine learning algorithms: a case study of the city of Melbourne, Australia. Sci Rep 13(1):13510

Atef I, Ahmed W, Abdel-Maguid RH (2023) Modelling of land use land cover changes using machine learning and GIS techniques: a case study in El-Fayoum Governorate, Egypt. Environ Monit Assess 195(6):637

Azabdaftari A, Sunar F (2022) District-based urban expansion monitoring using multitemporal satellite data: application in two mega cities. Environ Monit Assess 194(5):335

Bartesaghi-Koc C, Osmond P, Peters A (2022) Innovative use of spatial regression models to predict the effects of green infrastructure on land surface temperatures. Energy Build 254:111564

Bindajam AA, Mallick J, Hang HT (2023) Assessing landscape fragmentation due to urbanization in English Bazar Municipality, Malda, India, using landscape metrics. Environ Sci Pollut Res 30(26):68716–68731

Bindajam AA, Mallick J, AlQadhi S, Singh CK, Hang HT (2020) Impacts of vegetation and topography on land surface temperature variability over the semi-arid mountain cities of Saudi Arabia. Atmos 11(7):762

Chakraborti S, Banerjee A, Sannigrahi S, Pramanik S, Maiti A, Jha S (2019) Assessing the dynamic relationship among land use pattern and land surface temperature: a spatial regression approach. Asian Geogr 36(2):93–116

Chen H, Zhao Y, Fu X, Tang M, Guo M, Zhang S, ... Wu G (2022) Impacts of regional land-use patterns on ecosystem services in the typical agro-pastoral ecotone of Northern China. Ecosyst Health Sustain 8(1):2110521

Chughtai AH, Abbasi H, Karas IR (2021) A review on change detection method and accuracy assessment for land use land cover. Remote Sens Appl: Society and Environment 22:100482

Corumluoglu O (2023) Evaluation of the urban ecosystem and local climate changes caused by urbanization in İzmir in terms of long-term UHI formation with the SSI method. Resilience 7(1):11–58. https://doi.org/10.32569/resilience.1172781

Derdouri A, Wang R, Murayama Y, Osaragi T (2021) Understanding the links between LULC changes and SUHI in cities: insights from two-decadal studies (2001–2020). Remote Sens 13(18):3654

Dewa DD, Buchori I, Sejati AW, Liu Y (2022) Shannon entropy-based urban spatial fragmentation to ensure sustainable development of the urban coastal city: a case study of Semarang, Indonesia. Remote Sens Appl: Society and Environment 28:100839

Elfarkh J, Ezzahar J, Er-Raki S, Simonneaux V, Ait Hssaine B, Rachidi S, ... Jarlan L (2020) Multi-scale evaluation of the TSEB model over a complex agricultural landscape in Morocco. Remote Sens 12(7):1181

Ermida SL, Soares P, Mantas V, Göttsche FM, Trigo IF (2020) Google earth engine open-source code for land surface temperature estimation from the landsat series. Remote Sens 12(9):1471

Farid N, Moazzam MFU, Ahmad SR, Coluzzi R, Lanfredi M (2022) Monitoring the impact of rapid urbanization on land surface temperature and assessment of surface urban heat island using landsat in megacity (Lahore) of Pakistan. Front Remote Sens 3:897397

Furlan R, Marthya KL, Ellath LA, Esmat M, Al-Matwi R (2022) An urban regeneration-placemaking strategy for the Qatar National Museum and Souq Waqif's transit-oriented development in Doha, State of Qatar. J Urban Regen Renewal 16(2):182–206

Garg V, Anand A (2022) Impact of city expansion on hydrological regime of Rispana Watershed, Dehradun, India. Geojournal 87(Suppl 4):973–997

Gerace A, Kleynhans T, Eon R, Montanaro M (2020) Towards an operational, split window-derived surface temperature product for the thermal infrared sensors onboard Landsat 8 and 9. Remote Sens 12(2):224

Ghosh S, Kumar D, Kumari R (2022) Assessing spatiotemporal dynamics of land surface temperature and satellite-derived indices for new town development and suburbanization planning. Urban Governance 2(1):144–156

Gohain KJ, Goswami A, Mohammad P, Kumar S (2023) Modelling relationship between land use land cover changes, land surface temperature and urban heat island in Indore city of central India. Theoret Appl Climatol 151(3–4):1981–2000

Guha S, Govil H (2022) Annual assessment on the relationship between land surface temperature and six remote sensing indices using Landsat data from 1988 to 2019. Geocarto Int 37(15):4292–4311

Gunawardena KR, Wells MJ, Kershaw T (2017) Utilising green and bluespace to mitigate urban heat island intensity. Sci Total Environ 584:1040–1055

Guo G, Wu Z, Xiao R, Chen Y, Liu X, Zhang X (2015) Impacts of urban biophysical composition on land surface temperature in urban heat island clusters. Landsc Urban Plan 135:1–10

He BJ, Wang W, Sharifi A, Liu X (2023) Progress, knowledge gap and future directions of urban heat mitigation and adaptation research through a bibliometric review of history and evolution. Energy Build 112976

Hou J, Du Y (2020) Spatial simulation of rainstorm waterlogging based on a water accumulation diffusion algorithm. Geomat Nat Haz Risk 11(1):71–87

Hu Q, Zhang Z, Niu L (2022) Identification and evolution of territorial space from the perspective of composite functions. Habitat Int 128:102662

Ignatieva M, Stewart GH, Meurk C (2011) Planning and design of ecological networks in urban areas. Landscape Ecol Eng 7:17–25

Imran HM, Hossain A, Islam AS, Rahman A, Bhuiyan MAE, Paul S, Alam A (2021) Impact of land cover changes on land surface temperature and human thermal comfort in Dhaka city of Bangladesh. Earth Syst Environ 5:667–693

Jamali A (2020) Land use land cover mapping using advanced machine learning classifiers: a case study of Shiraz city, Iran. Earth Sci Inform 13(4):1015–1030

Kabir S, Pahlevan N, O'Shea RE, Barnes BB (2023) Leveraging Landsat-8/-9 underfly observations to evaluate consistency in reflectance products over aquatic environments. Remote Sens Environ 296:113755

Kaiser, E. A., Rolim, S. B. A., Grondona, A. E. B., Hackmann, C. L., de Marsillac Linn, R., Käfer, P. S., ... & Diaz, L. R. (2022). Spatiotemporal Influences of LULC changes on land surface temperature in rapid urbanization area by using Landsat-TM and TIRS images. *Atmosphere, 13*(3), 460.

Kim M, Kim D, Kim G (2022) Examining the relationship between land use/land cover (LULC) and land surface temperature (LST) using explainable artificial intelligence (XAI) models: a case study of Seoul, South Korea. Int J Environ Res Public Health 19(23):15926

Kotrosits M (2013) Affect, violence, and belonging in early Christianity. PhD. Diss., Union Theol Seminary

Krivoguz D, Chernyi SG, Zinchenko E, Silkin A, Zinchenko A (2023) Using Landsat-5 for accurate historical LULC classification: a comparison of machine learning models. Data 8(9):138

Lal P, Dubey AK, Kumar A, Kumar P, Dwivedi CS (2022) Measuring the control of landscape modifications on surface temperature in India. Geocarto Int 37(27):15736–15753

Li W, Bai Y, Chen Q, He K, Ji X, Han C (2014) Discrepant impacts of land use and land cover on urban heat islands: a case study of Shanghai, China. Ecol Ind 47:171–178

Li Z, Wang F, Kang T, Wang C, Chen X, Miao Z, ... Zhang H (2022) Exploring differentiated impacts of socioeconomic factors and urban forms on city-level CO2 emissions in China: spatial heterogeneity and varying importance levels. Sustain Cities Soc 84:104028

Li ZL, Wu H, Duan SB, Zhao W, Ren H, Liu X, ... Zhou C (2023) Satellite remote sensing of global land surface temperature: definition, methods, products, and applications. Rev Geophys 61(1):e2022RG000777

Lin J, Qiu S, Tan X, Zhuang Y (2023) Measuring the relationship between morphological spatial pattern of green space and urban heat island using machine learning methods. Build Environ 228:109910

Loukika KN, Keesara VR, Sridhar V (2021) Analysis of land use and land cover using machine learning algorithms on google earth engine for Munneru River Basin, India. Sustainability 13(24):13758

Mahmood R, Pielke Sr RA, Hubbard KG, Niyogi D, Dirmeyer PA, McAlpine C, ... Fall S (2014) Land cover changes and their biogeophysical effects on climate. Int J Climatol 34(4):929–953

Malanson GP, Alftine KJ (2023) Ecological impacts of climate change. In Biological and Environmental Hazards, Risks, and Disasters (pp. 449–479). Elsevier

Mallick J, Kant Y, Bharath BD (2008) Estimation of land surface temperature over Delhi using Landsat-7 ETM+. J Ind Geophys Union 12(3):131–140

Mendes CB, Prevedello JA (2020) Does habitat fragmentation affect landscape-level temperatures? A global analysis. Landscape Ecol 35:1743–1756

Moazzam MFU, Doh YH, Lee BG (2022) Impact of urbanization on land surface temperature and surface urban heat Island using optical remote sensing data: a case study of Jeju Island, Republic of Korea. Build Environ 222:109368

Mohamed A, Worku H, Lika T (2020) Urban and regional planning approaches for sustainable governance: The case of Addis Ababa and the surrounding area changing landscape. City Environ Interact 8:100050

Moisa MB, Dejene IN, Gemeda DO (2022) Integration of geospatial technologies with multiple regression model for urban land use land cover change analysis and its impact on land surface temperature in Jimma City, southwestern Ethiopia. Appl Geomatics 14(4):653–667

Mokarram M, Taripanah F, Pham TM (2023) Investigating the effect of surface urban heat island on the trend of temperature changes. Adv Space Res 72(8):3150–3169

Mukherjee F, Singh D (2020) Assessing land use–land cover change and its impact on land surface temperature using LANDSAT data: a comparison of two urban areas in India. Earth Syst Environ 4:385–407

Naikoo MW, Rihan M, Ishtiaque M (2020) Analyses of land use land cover (LULC) change and built-up expansion in the suburb of a metropolitan city: spatio-temporal analysis of Delhi NCR using landsat datasets. J Urban Manag 9(3):347–359

Naikoo MW, Islam ARMT, Mallick J, Rahman A (2022a) Land use/land cover change and its impact on surface urban heat island and urban thermal comfort in a metropolitan city. Urban Climate 41:101052

Naikoo MW, Rihan M, Shahfahad Peer AH, Talukdar S, Mallick J, ... Rahman A (2022b) Analysis of peri-urban land use/land cover change and its drivers using geospatial techniques and geographically weighted regression. Environ Sci Pollut Res 1–19

Namgyal T, Thakur DA, Rishi DS, Mohanty MP (2023) Are open-source hydrodynamic models efficient in quantifying flood risks over mountainous terrains? An exhaustive analysis over the Hindu-Kush-Himalayan region. Sci Total Environ 897:165357

Nath B, Ni-Meister W, Choudhury R (2021) Impact of urbanization on land use and land cover change in Guwahati city, India and its implication on declining groundwater level. Groundw Sustain Dev 12:100500

Ouma Y, Nkwae B, Moalafhi D, Odirile P, Parida B, Anderson G, Qi J (2022) Comparison of machine learning classifiers for multitemporal and multisensor mapping of urban LULC features. Int Arch Photogramm Remote Sens Spat Inf Sci 43:681–689

Pande CB, Moharir KN, Varade AM, Abdo HG, Mulla S, Yaseen ZM (2023) Intertwined impacts of urbanization and land cover change on urban climate and agriculture in Aurangabad city (MS), India using Google Earth Engine platform. J Clean Prod 422:138541

Phelps NA, Nichols D (2022) Can growth be planned? The case of melbourne's urban periphery. J Plan Educ Res. https://doi.org/10.1177/0739456X221121248

Rahaman ZA, Kafy AA, Saha M, Rahim AA, Almulhim AI, Rahaman SN, ... Al Rakib A (2022) Assessing the impacts of vegetation cover loss on surface temperature, urban heat island and carbon emission in Penang city, Malaysia. Build Environ 222:109335

Rihan M, Bindajam AA, Talukdar S, Naikoo MW, Mallick J, Rahman A (2023) Forest fire susceptibility mapping with sensitivity and uncertainty analysis using machine learning and deep learning algorithms. Adv Space Res 72(2):426–443

Roy S, Pandit S, Eva EA, Bagmar MSH, Papia M, Banik L, ... Razi MA (2020) Examining the nexus between land surface temperature and urban growth in Chattogram Metropolitan Area of Bangladesh using long term Landsat series data. Urban Clim 32:100593

Saleem MS, Ahmad SR, Javed MA (2020) Impact assessment of urban development patterns on land surface temperature by using remote sensing techniques: a case study of Lahore, Faisalabad and Multan district. Environ Sci Pollut Res 27(32):39865–39878

Salvati L, Zambon I, Chelli FM, Serra P (2018) Do spatial patterns of urbanization and land consumption reflect different socioeconomic contexts in Europe? Sci Total Environ 625:722–730

Sarkar SK, Talukdar S, Rahman A et al (2021) Groundwater potentiality mapping using ensemble machine learning algorithms for sustainable groundwater management. Front Eng Built Environ 2:43–54

Sekertekin A, Bonafoni S (2020) Land surface temperature retrieval from Landsat 5, 7, and 8 over rural areas: assessment of different retrieval algorithms and emissivity models and toolbox implementation. Remote Sens 12(2):294

Seyam MMH, Haque MR, Rahman MM (2023) Identifying the land use land cover (LULC) changes using remote sensing and GIS approach: a case study at Bhaluka in Mymensingh, Bangladesh. Case Stud Chem Environ Eng 7:100293

Shahfahad, Talukdar S, Rihan M, Hang HT, Bhaskaran S, Rahman A (2021) Modelling urban heat island (UHI) and thermal field variation and their relationship with land use indices over Delhi and Mumbai metro cities. Environ Dev Sustain 0123456789. https://doi.org/10.1007/s10668-021-01587-7

Shahfahad Bindajam AA, Naikoo MW, Horo JP, Mallick J, Rihan M, ... Rahman A (2023a) Response of soil moisture and vegetation conditions in seasonal variation of land surface temperature and surface urban heat island intensity in sub-tropical semi-arid cities. Theor Appl Climatol 1–29

Shahfahad Bindajam AA, Naikoo MW, Talukdar S, Asif Mallick J, Rahman A (2023b) Analysing diurnal temperature range and extreme temperature events over Delhi and Mumbai mega cities. Natural Hazards 1–29

Shen C, Hou H, Zheng Y, Murayama Y, Wang R, Hu T (2022) Prediction of the future urban heat island intensity and distribution based on landscape composition and configuration: a case study in Hangzhou. Sustain Cities Soc 83:103992

Shetty S (2019) Analysis of machine learning classifiers for LULC classification on Google Earth Engine (Master's thesis, University of Twente)

Singh RK, Singh P, Drews M, Kumar P, Singh H, Gupta AK, ... Kumar M (2021) A machine learning-based classification of LANDSAT images to map land use and land cover of India. Remote Sens Appl: Society and Environment 24:100624

Srikanth K, Swain D (2022) Urbanization and land surface temperature changes over Hyderabad, a semi-arid mega city in India. Remote Sens Appl: Society and Environment 28:100858

Srivastava A, Bharadwaj S, Dubey R, Sharma VB, Biswas S (2022) Mapping vegetation and measuring the performance of machine learning algorithm in LULC classification in the large area using Sentinel-2 and Landsat-8 datasets of Dehradun as a test case. Int Arch Photogramm Remote Sens Spat Inf Sci 43:529–535

Su H, Han G, Li L, Qin H (2021) The impact of macro-scale urban form on land surface temperature: an empirical study based on climate zone, urban size and industrial structure in China. Sustain Cities Soc 74:103217

Sumanta DAS (2022) A review of urban heat island formation over changing climate and its impacts on urban land use and environments and adaptation measures. Int J Environ Geoinform 9(1):64–73

Talukdar S, Singha P, Mahato S, Pal S, Liou YA, Rahman A (2020) Land-use land-cover classification by machine learning classifiers for satellite observations—a review. Remote Sens 12(7):1135

Talukdar S, Eibek KU, Akhter S, Ziaul SK, Islam ARMT, Mallick J (2021) Modeling fragmentation probability of land-use and land-cover using the bagging, random forest and random subspace in the Teesta River Basin, Bangladesh. Ecol Indic 126:107612

Tan J, Yu D, Li Q, Tan X, Zhou W (2020) Spatial relationship between land-use/land-cover change and land surface temperature in the Dongting Lake area, China. Sci Rep 10(1):9245

Tang H, Yan X, Liu T, Zheng J (2023) Spatio-temporal evolution of urban expansion along suburban railway lines in megacities based on multi-source data: a case study of Beijing, China. Remote Sens 15(19):4684

Thakur S, Maity D, Mondal I, Basumatary G, Ghosh PB, Das P, De TK (2021) Assessment of changes in land use, land cover, and land surface temperature in the mangrove forest of Sundarbans, northeast coast of India. Environ Dev Sustain 23:1917–1943

Tian Y, Tsendbazar NE, van Leeuwen E, Fensholt R, Herold M (2022) A global analysis of multifaceted urbanization patterns using Earth Observation data from 1975 to 2015. Landsc Urban Plan 219:104316

Tsagkatakis G, Aidini A, Fotiadou K, Giannopoulos M, Pentari A, Tsakalides P (2019) Survey of deep-learning approaches for remote sensing observation enhancement. Sensors 19(18):3929

Varade D, Singh H, Singh AP, Awasthi S (2023) Assessment of urban sprawls, amenities, and indifferences of LST and AOD in sub-urban area: a case study of Jammu. Environ Sci Pollut Res 30(49):107179–107198

Wang F, Qin Z, Song C, Tu L, Karnieli A, Zhao S (2015) An improved mono-window algorithm for land surface temperature retrieval from Landsat 8 thermal infrared sensor data. Remote Sens 7(4):4268–4289

Wang Y, Wang D, Geng N, Wang Y, Yin Y, Jin Y (2019) Stacking-based ensemble learning of decision trees for interpretable prostate cancer detection. Appl Soft Comput 77:188–204

Wang R, Hou H, Murayama Y, Derdouri A (2020) Spatiotemporal analysis of land use/cover patterns and their relationship with land surface temperature in Nanjing, China. Remote Sens 12(3):440

Wang J, Bretz M, Dewan MAA, Delavar MA (2022) Machine learning in modelling land-use and land cover-change (LULCC): current status, challenges and prospects. Sci Total Environ 822:153559

Wu W, Zhi C, Gao Y, Chen C, Chen Z, Su H, ... Tian B (2022) Increasing fragmentation and squeezing of coastal wetlands: status, drivers, and sustainable protection from the perspective of remote sensing. Sci Total Environ 811:152339

Wulder MA, Coops NC, Roy DP, White JC, Hermosilla T (2018) Land cover 2.0. Int J Remote Sens 39(12):4254–4284

Xu C, Lin M, Fang Q, Chen J, Yue Q, Xia J (2023) Air temperature estimation over winter wheat fields by integrating machine learning and remote sensing techniques. Int J Appl Earth Obs Geoinf 122:103416

Yang Z, Huang Y, Duan Z, Tang J (2023) Capturing the spatiotemporal variations in the gross primary productivity in coastal wetlands by integrating eddy covariance, Landsat, and MODIS satellite data: a case study in the Yangtze Estuary, China. Ecol Indic 149:110154

Yang H, Xi C, Zhao X, Mao P, Wang Z, Shi Y, ... Li Z (2020) Measuring the urban land surface temperature variations under Zhengzhou city expansion using Landsat-like data. Remote Sens 12(5):801

Yao Y, Sun Z, Li L, Cheng T, Chen D, Zhou G, ... Guan Q (2023) CarbonVCA: A cadastral parcel-scale carbon emission forecasting framework for peak carbon emissions. Cities 138:104354

Yonaba R, Mounirou LA, Tazen F, Koïta M, Biaou AC, Zouré CO, ... Yacouba H (2023) Future climate or land use? Attribution

of changes in surface runoff in a typical Sahelian landscape. Comptes Rendus. Géoscience 355(S1):1–28

Zhang S, Yang D, Yang Y, Piao S, Yang H, Lei H, Fu B (2018) Excessive afforestation and soil drying on China's Loess Plateau. J Geophys Res Biogeosci 123(3):923–935

Zhang Y, Wang Y, Ding N (2022) Spatial effects of landscape patterns of urban patches with different vegetation fractions on urban thermal environment. Remote Sens 14(22):5684

Zhao ZQ, He BJ, Li LG, Wang HB, Darko A (2017) Profile and concentric zonal analysis of relationships between land use/land cover and land surface temperature: case study of Shenyang, China. Energy Build 155:282–295

Zhou W, Huang G, Cadenasso ML (2011) Does spatial configuration matter? Understanding the effects of land cover pattern on land surface temperature in urban landscapes. Landsc Urban Plan 102(1):54–63

Zhou W, Qian Y, Li X, Li W, Han L (2014) Relationships between land cover and the surface urban heat island: seasonal variability and effects of spatial and thematic resolution of land cover

data on predicting land surface temperatures. Landscape Ecol 29:153–167

Zhou W, Wang J, Cadenasso ML (2017) Effects of the spatial configuration of trees on urban heat mitigation: a comparative study. Remote Sens Environ 195:1–12

Zhou Y, Chen T, Feng Z, Wu K (2022) Identifying the contradiction between the cultivated land fragmentation and the construction land expansion from the perspective of urban-rural differences. Eco Inform 71:101826